Milankovitch frequencies in tephra records at volcanic arcs: The relation of kyr-scale cyclic variations in volcanism to global climate changes

S. Kutterolf[1], J.C. Schindlbeck[2], M. Jegen[1], A. Freundt[1], S.M. Straub[3]

[1]GEOMAR Helmholtz Centre for Ocean Research Kiel, 24148 Kiel, Germany

[2]University of Heidelberg Institute of Earth Sciences, 69120 Heidelberg, Germany

[3]Lamont Doherty Earth Observatory Columbia University, Palisades, USA

Abstract

The increase in volcanic activity after the last glacial maximum observed on Iceland has led to one of the most fascinating hypothesis in science in the last decades: that deglaciation may force volcanism. Consequently, tephrostratigraphic records of sufficient length that cover multiple glacial cycles have been used to test whether such relationships hold systematically through the Quaternary. Here we review such tephra records that have been linked with climate proxy records such as $\delta^{18}O$ in marine sediments, which is a measure of sea-level change and which is thought to be orbitally forced, as it exhibits the characteristic Milankovitch periodicities of precession (~23 kyr), obliquity (~41 kyr) and eccentricity (~100 kyr).

Statistical analyses have identified these periodicities also in long tephra records from different latitudes and geotectonic settings, as well as in compiled semi-global records. These studies detect Milankovitch periods in their tephra record, and also a phase shift relative to the $\delta^{18}O$ record in such that periods of increased eruption frequencies coincide with the deglaciation period at the glacial/interglacial transition when ice and water loads on the lithosphere change most rapidly. However, there are also disparities in results and interpretations, which may be attributable to the different methods of analysis applied the studies.

We have therefore re-analyzed the four best-characterized tephra records by the same methods. We distinguish between analysis in the frequency domain, a novel approach, and analysis in the time domain, which has been used in previous studies. Analysis in the frequency domain identifies harmonic frequencies that arise from the binary nature of the tephra records and complicate the identification of primary frequencies. However, we show that all four records show spectral density peaks near the main Milankovitch periodicities of 41 and 100 kyr, and that they produce meaningful and significant statistical correlations with each other and the global $\delta^{18}O$ record but not with random time series. Although the time-domain correlations with $\delta^{18}O$ roughly confirm phase shifts implying peak volcanism during deglaciation, correlation coefficients arising from very noisy records are generally too low for precise constraints on the relative timing.

These deficiencies presently hamper the recognition of the physical mechanisms through which global climate changes affect volcanism at both, high-latitude glaciated regions and low-latitude non-glaciated regions.

Keywords: Quaternary, eruption frequencies, cyclicities, climate, tephra time series, Milankovitch, statistics

Introduction

It is well known that large explosive and effusive eruptions can have a global impact on the climate through the injection of gas, aerosols and ash into the atmosphere which can reduce average global surface temperature over a period of years (McCormick et al., 1995; Robock, 2000; Miller et al., 2012). Some of these volcanic impacts led to widespread droughts, crop losses, and famine causing dramatic casualties (e.g., Oppenheimer, 2003; Lavigne et al., 2013, Manning et al. 2017). The most prominent historic examples are the 1783-1784 Laki eruption on Iceland (e.g., Highwood and Stevenson, 2003), the 1815 Tambora eruption in Indonesia (e.g., Rampino et al., 1993; Rampino and Self, 1982) and the 1991 Mt. Pinatubo eruption on the Philippines (e.g., Robock, 2000). Modern global measurement networks (for example, see www.ncdc.noaa.gov) nowadays demonstrate the climatic effects of volcanic eruptions, but for events in the distant past these relationships need to be revealed by correlating volcanic and paleoclimate records. For example, tree rings of the last 600 years record excursions in the average northern hemisphere surface temperatures that can be related to large volcanic eruptions during this period (Briffa et al. 2004) (Fig.1). Sigl et al. (2015) correlated Arctic and Antarctic ice core data and lower latitude climate proxy records (such as tree cores) and identified global climate forcings by volcanic events over the past 2500 years. On time scales of tens of million years, geologic records reveal mass extinctions caused by the severe climate disruption associated with formation of large igneous provinces and flood basalts (Hofmann et al., 1997; McLean, 1985; Campbell et al., 1992; Courtillot and Renne, 2003; Bond and Wignall, 2014).

However, there is also another way to assess the relationships between paleoclimate and volcanic records. Over past decades it has been recognized that variations in global climate and in volcanic activity share some common periodicities, also known as the Milankovitch periods, which led to the theory that global climate changes may be a driver of volcanic activity (Paterne et al., 1990; Rampino et al., 1979). Cyclic behavior of volcanoes and volcanic provinces can occur on a wide range of timescales, from seconds over hours and days up to millions of years (e.g., Table 1, Carey and Sigurdsson, 2000; Sigurdsson et al. 2000, Kutterolf et al. 2013; Sumita and Schmincke, 2013; Scharff et al., 2015; Bredemeyer and Hansteen, 2014; Schindlbeck et al., 2015, 2018; Tolstoy, 2015; Mahony et al., 2016). The reasons for such temporal variations in volcanic activity can be internal drivers in volcano-magma systems (e.g., mantle melting rates, magma storage and replenishment conditions, or degassing processes) or external influences such as regional earthquakes, seasonal climate variations, Earth tides, regional sea-level changes or ocean tides, or regional tectonic rearrangements (e.g., Table 1; Schmincke, 2004; Johnston and Mauk, 1972; Dzurizin, 1980; McNutt and Beavan, 1987; Patanè et al., 1994; Mason et al., 2004; Sottili et al., 2007; Kasahara and Sato, 2001 Bredemeyer and Hansteen, 2014; Tolstoy, 2015; Mahony et al., 2016). Sealevel change has in particular been invoked as an external control on volcanism. For example, Steward (2018) links the sudden change from fissure-type to central-type volcanism at Mt. Etna to a dramatic sealevel rise. Sternai et al. (2017) propose that the dramatic sealevel drop of the Messinian salinity crisis increased the productivity of the pan-Mediterranean volcanic provinces. Jupp et al. (2004) developed a theoretical model to predict possible distributions of response times of volcanism depending on magnitude and frequency of a periodic stimulation.

Studies in Iceland (Sigvaldason et al., 1992; MacLennan et al., 2002) and other glacier-covered regions (e.g., Praetorius et al., 2016; Rawson et al., 2016) showed a significant increase in volcanic activity after the last glaciation, suggesting that lithospheric unloading during glacier retreat may drive volcanism. Theoretical modeling by Jull and McKenzie (1996) confirms that glacier unloading can significantly increase mantle melting at Iceland. Nowell et al. (2006) observed increased volcanic activity in young intraplate volcanic fields in France and Germany during post-glacial warming periods and related this to distal effects of flexural (un-)loading of the lithosphere in response to ice shield retreat.

A globally applicable proxy of global climate variations is the foraminiferal $\delta^{18}O$ record, which provides a measure of global ice volume and sea level change (Lisiecki and Raymo, 2005). The $\delta^{18}O$ record, as well as some other paleoclimate proxy records, contains cyclic variations on periods that reflect orbital forcing of the climate (Milankovitch cycles), of which the most prominent are precession (23 kyr) and obliquity (41 kyr) of Earth's rotation axis, and the eccentricity (100 kyr) of Earth's rotation around the sun; minor periodicities occur at 17-19 kyr and 400 kyr. The fact that the major periodicities have also been recognized in various volcanic records in geodynamic settings (Fig. 2) gave rise to the hypothesis that climate change drives volcanism (e.g. McGuire et al. 1997, Jellinek et al. 2004, Huybers and Langmuir, 2009; Kutterolf et al. 2013, Schindlbeck et al. 2018). In this review we address the results as well as commonalities and disparities between the various studies of climate-volcanism relationships in order to provide a better basis for deducing the physical mechanisms of that relationship, which remain poorly understood and for which different processes have been suggested. Understanding such mechanisms is relevant to the present-day because anthropogenically enforced deglaciation may lead to increased volcanic activity and hazards (Tuffen, 2010; Pagli and Sigmundsson, 2008; Albino et al., 2010).

Volcanic time series

The geologic investigation of volcanic systems on land is the most common way to reconstruct time series of volcanic activity, typically involving a large number of radiometric datings (e.g., Glazner et al., 1999; Nowell et al., 2006). Coverage by younger deposits, erosion, or other reasons may render parts of the volcanic history inaccessible. Kiyosugi et al. (2015) found an exponential trend of under-recording of explosive eruptions with age in Quaternary Japanese tephra records, with stronger under-recording of smaller eruptions. However, the mostly non-erosive conditions in lakes or on the ocean floor facilitate the recovery of medial to distal tephra records that approximate a continuous history of regional (e.g., Paterne et al., 1990), and even global-scale volcanism (Kutterolf et al., 2013) (Table 1). It can be assumed that the temporal variation in the frequency of explosive eruptions that produce widespread tephra beds is an image of the temporal variation of the entire volcanism because it has been shown that eruption magnitude and frequency are systematically linked to each other (e.g. Pyle, 1995; Deligne et al., 2010). An advantage of sedimentary tephra profiles is that there are often independent (mostly micropaleontological) methods to establish high-resolution age models, a prequisit to further study the time series statistical. Most of the studies that investigate volcanic time series for Milankovitch frequencies build indeed on tephra successions, and in this review we will further focus on results from marine tephra sequences.

However, it should be noted that correlations with climate signals have also been observed in other volcanic records. For example, variations in crustal thicknesses in seafloor bathymetry suggest a sensitivity of mid-ocean ridge systems to sea level changes on Milankovitch time scales (e.g., Table 1; Tolstoy, 2015; Lund et al., 2011; Crowley et al., 2015). Moreover, the peak of hydrothermal activity on the Mid-Atlantic Ridge (Middleton et al., 2016), Juan de Fuca Ridge (Costa et al., 2017) and at the East Pacific Rise (Lund et al., 2016) ~15 kyr after the glacial maximum has been interpreted as the delayed melt formation following the hydrostatic pressure minimum.

The tephra time series can be distinguished into two categories: tephra successions that cover single volcanic systems, or volcanic provinces (e.g., Paterne et al., 1990; Schindlbeck et al., 2018), and compiled tephra records that include data from many sites in order to approximate a semi-global tephra record (e.g., Huybers and

Langmuir, 2009; Kutterolf et al., 2013) (Table 1). Both types of data sets can represent different age ranges. We will first summarize studies that investigate tephra records since the last glaciation; these records are best accessible and provide the best available time resolution. In a subsequent chapter we then discuss tephra record spanning several glacial cycles as only these can provide a conclusive test of the proposed climate-volcanism relationships.

Tephra studies covering the last glacial cycle

Especially in glaciated regions (e.g. Chile, Iceland, Alaska) several studies found an increase in volcanic activity during the last deglaciation (e.g., Table 1; Praetorius et al., 2016; Rawson et al., 2016; Sigvaldason et al., 1992; MacLennan et al., 2002). In a combined tephra and lava study on Iceland, Sigvaldason et al. (1992) inferred that ice unloading increased post-glacial magma production rates and eruptability of Icelandic magmas following the last deglaciation. They note that a major problem is the sampling and volume determination of layers that are buried under younger deposits as well as the limitation of their data to the last deglaciation.

Figure 3a shows the temporal evolution of ice volume equivalent sea-level variation across the last glaciation after Lambeck et al. (2014). Sea-level rise during deglaciation is not steady but shows a significant pulse (meltwater pulse 1a, orange box in Fig. 3a) during the Bølling-Allerød period. Interestingly, this pulse is almost immediately followed by the period of postglacial rebound in Iceland (gray bar in Fig. 3a; MacLennan et al., 2002). The phase of increased postglacial volcanism in Iceland largely overlaps with the postglacial rebound and the meltwater pulse (Fig. 3b). Similarly, on the other side of the planet, the high-resolution postglacial volcanic activity of Mocho-Choshuenco volcano at the glaciated southern Chilean arc (Rawson et al., 2016) peaks during the same 13-8 ka period (Fig 3b). Rawson et al.

(2016) attributed this to changes in magma storage times that are caused by deglaciation-related changes in the crustal stress field. They suggest that magma is stored during the glaciation and erupts in a first explosive phase immediately after the ice unloading. Praetorius et al. (2016) observed an abrupt increase in the volcanic activity at the Mt. Edgecumbe Volcanic Field in Southeast Alaska between 14.6 and 13.1 ka, which coincides with the period of largest crustal uplift in response to glacial ablation (Fig. 3c). Note that there is a time shift of about 2000 years in peak rebound and peak volcanism between Alaska and Iceland.

A global increase of volcanic activity during the last deglaciation is also discussed. In a 40 kyr compilation of subaerial eruptions from different latitudes Huybers and Langmuir (2009) noticed an increase of volcanic activity during the last deglaciation (12-7 ka) and into the Holocene that largely coincides with the period of high sea-level stand (Fig. 3d). However, Watt et al. (2013) revised the work of Huybers and Langmuir by distinguishing between glaciated and non-glaciated arc regions. They conclude that the apparent increase in global volcanism during the last deglaciation is mainly due to an increase in volcanism in glaciated regions.

Huybers and Langmuir (2009) and Praetorius et al. (2016) speculated that increased volcanism may create a positive feedback on deglaciation by adding CO_2 to the atmosphere and by reduction of the albedo by ash mantling the ice sheets.

Tephra studies on longer time scales

The longest tephra records, covering up to 35 Myr, have been documented by Kennett and Thunell (1975), and Kennett et al. (1977) who use the time distribution of volcanic ash in 320 Tertiary to Recent deep-drilled sequences obtained by the Deep Sea Drilling Project (DSDP) in combination with terrestrial data (Fig. 4). These data were complemented by Cadet et al. (1982a,b) offshore Central America and by

Carey and Sigurdsson (2000) and Sigurdsson et al. (2000) for the Caribbean region (Fig.4; Table 1). These studies identified several widely occurring cycles in volcanic activity that each lasted several million years and which can be attributed to plate tectonic processes. However, these tephra records did not have the temporal resolution necessary to identify cyclic variations in the 10's of kyr range. Prueher and Rea (2001) obtained a higher resolution tephra record (450 ash beds in 5 Myr) from the northern Pacific and detected episodes of increased explosive volcanism at approximately 0.2–0.5, 0.7–0.9, 1.5–1.7, and 2.5–2.65 Ma in the Kamchatka arc, and at 0.15–0.4, 1.7–1.8, 2.55–2.65, and at 3.0–3.1 Ma in the eastern Aleutian arc. These periods correspond to those found throughout the Pacific (e.g., Cambray et al., 1995) (Fig. 4). Prueher and Rea (1998) emphasize the synchronism of the ~2.5 Ma intense volcanic period all around the North Pacific and agree with Cambray et al. (1995) who suggest that the underlying mechanism operated on a much larger scale than just a local change in subduction angle or rate. They suggest a link between intense volcanism and Late Pliocene glaciation. Kennett et al. (1975) already hypothesized that climatic (e.g., late Pliocene glaciation) rather than tectonic controls forced periods of enhanced volcanic activity, but were unable to demonstrate this. In the following we focus on studies that employed statistical methods to analyze volcanic time series and their correlation with paleo-climate time series.

Paterne et al. (1990) studied the 190 kyr volcanic history of the Campanian province (Italy) through the tephra inventory of central Mediterranean marine sediment cores. Tephra layers were correlated between cores and dated by $\delta^{18}O$ stratigraphy as well as through correlation with dated tephras on land, providing a total of 151 volcanic events (118 Campanian, 33 from other Italian volcanic systems). Using a sliding-window technique, Paterne et al. (1990) generated a frequency distribution over time that revealed five periods of enhanced volcanic activity (Fig. 5), which correlate with compositional changes in the volcanic rocks. Moreover, power spectral analysis shows that these pulses occur with a 23 kyr periodicity, which is close to the Earth's precession period.

McGuire et al. (1997) compiled an 80 kyr long succession of ash layers of the central and eastern Mediterranean Sea including also the time series of Paterne et al. (1990). They observed enhanced tephra accumulation at 8–15, 34–38, and 55–61 kyr BP and compared these intervals with the paleo-sea-level record. They applied statistical methods to analyze the time series and noted that the around 22 kyr period of relative volcanic quiescence correlates with the last low sea-level stand while the volcanically intense period 8–15 kyr accompanied the very rapid post-glacial sea-level rise (Fig. 5). By determining the first derivative of the sea-level variation McGuire et al. (1997) showed that tephra frequency correlates with the rate of sea-level change but lags behind by a few thousand years.

Glazner et al. (1999) investigated the distribution of radiometric ages of intraplate volcanic events in eastern California over the last 800 kyr. Their smoothed age distribution shows peaks at 10, 100, 185, 320 and 690 kyr, which visually anticorrelate with interglacial maxima (Fig. 6). Subsequently, Jellinek et al. (2004) statistically evaluated the first 400 kyr of the data set by 1) distinguishing between basaltic and silicic volcanism, and 2) calculating power spectra for this volcanic time series as well as for a comparative climate time series (SPECMAP) that serves as a proxy for global glaciation (e.g., Shackleton, 1987), using a standard multi-taper algorithm (Fig. 7a, b). They found a clear 40 kyr and less-well constrained 17 and 23 kyr periodicities (i.e., the well-known Milankovitch periods) in the volcanic record as well as in the SPECMAP climate proxy data. Their advanced statistical treatment also revealed a significant correlation between changes in eruption frequency and the first derivative of the glacial time series, suggesting a response of volcanism to the rate of ice-volume reduction that occurs with a time lag of 3.2 ± 4.2 kyr for silicic, and 11.2 ± 2.3 kyr for basaltic magmas, respectively.

Schindlbeck et al. (2018) statistically analyzed the 1.1 Myr long tephra record of IODP Hole U1437B at the Izu-Bonin arc (IB) and its relation to a) the planktonic foraminifera $\delta^{18}O$ profile of the core, and to b) the global benthic foraminifera $\delta^{18}O$ reference stack of Lisiecki and Raymo (2005) as climate and sea level proxy (Fig. 6). Spectral analysis of the tephra dataset yields a statistically significant spectral peak at the ~100 kyr period (the Milankovitch eccentricity period), which dominates global climate cycles since the Middle Pleistocene (Fig. 7c, d). A time-domain analysis of the tephra and $\delta^{18}O$ records shows that volcanism peaks approximately 7 kyr after the glacial maximum, which coincides with the period of the fastest rate of lithospheric pressure change generated by deglaciation.

At Site U1437B, the best tephra- $\delta^{18}O$ correlation obtained for the last 0.7 Myr. The quality of the correlation is less for the period 0.7 – 1.1 Ma, also known as the Middle Pleistocene Transition (MPT), a period during which the climate signal, expressed as $\delta^{18}O$, the gradually changes from a 40 kyr dominant frequency to the 100 kyr frequency (Fig. 7). Despite the decrease in spectral density of the 100 kyr periodicity in the $\delta^{18}O$ record during the MPT, the tephra record maintains its dominant 100 kyr periodicity. Since this periodicity is associated with the formation of huge Northern hemisphere continental ice sheets (Mudelsee and Schulz, 1997), Schindlbeck et al. (2018) conclude that ice sheet formation persistent through the MPT, yet its 100 kyr periodicity in the $\delta^{18}O$ spectrum is largely obscured due to interference with other, shorter periodicities. Differences in the correlation between volcanism and $\delta^{18}O$ record across the MPT were also observed by Nowell et al. (2006) in their analysis of the 2 Myr eruption record of the western European volcanic fields. They note that correlation results would be biased by the higher abundance of volcanic events associated with higher oxygen isotope levels at <800 ka. However, comparison of volcanic events with the contemporary slope in $\delta^{18}O$ yielded best correlations as volcanic activity lagged maximum warming rate 3-6 kyr.

While the above studies focused on geographically and geotectonically limited regions, Kutterolf et al. (2013) compiled a tephra record from marine drill sites around the entire Pacific Ring of Fire (ROF) (Fig. 6). This tephra record is assumed to approximate the global temporal variation in eruption frequencies, since the ROF accounts for about half of the global length of active plate subduction. Spectral analysis identified a strong spectral peak for the obliquity period (41 kyr), while the other Milankovitch periods are less significant or absent in that tephra record (Fig. 7e). Kutterolf et al. observed excellent correlation between the tephra record and the first derivative of the $\delta^{18}O$ record with a time lag of 4.0 ± 3.6 kyr, i.e. highest frequency of volcanic eruptions is associated with the highest rate of rising eustatic sea level (decreasing global ice volume). Numerical simulations quantify how changes in eustatic sea level and glacial loading induced near-surface stress variations during the last glacial cycle (Kutterolf et al., 2013). For Central America, the most detailed ROF tephra record, maximum eruption frequency coincides with the time of maximum rate of lithostatic pressure change after the last glaciation.

The baseline derived from these diverse regional and global studies is that periodic pulses of volcanic activity are observed and that these periodicities correlate with the Milankovitch periodicities of the global sea-level ($\delta^{18}O$) record with a certain phase shift. However, the periodicities recognized differ between the tephra records, and no tephra record contains the entire set of Milankovitch periodicities. These differences, which may arise from the different lengths and event densities of the tephra records, make it difficult to identify the underlying driving mechanisms by which climate affects volcanic frequencies. We will further discuss these subjects in the following sections.

Discussion

While the studies summarized above all agree that global climate changes affect volcanism and typically lead to increased volcanism during deglaciation, there are also significant differences in the results (Table 1). For example, does peak volcanism correlate with absolute sea-level/glaciation variations or with the rate of change of sea-level? Why does each tephra record contain a different subset of the Milankovitch periodicities? Why do the observed time lags in the volcanism-climate correlations vary significantly? We now discuss two important issues that may be responsible for the different results:

1) the nature of tephra time series, and

2) the methods of statistical treatment.

Understanding these aspects is important for deducing the physical mechanisms through which climate changes may force volcanism.

The nature of tephra time series

The tephra time series are largely based on drill cores, in some cases also involving data from geologic field studies. Uncompacted to little compacted sediments are typically cored by gravity or piston coring including APC (advanced piston coring) employed during deep sea drilling. These methods usually provide mostly full (100%) recovery so that late Pleistocene through Holocene sequences can be recovered almost completely. Harder rocks typically in deeper core sections require rotary drilling, which yields much less recovery. Moreover, in highly compacted, altered and cemented rocks the recognition of thin ash beds can become difficult, especially when mineral-glass transitions as well as secondary mineral growth modify the sediment and obscure tephra signals. Therefore early Quaternary to Tertiary tephra sequences are expected to yield a lower event frequency. An increasing under-representation of volcanic events with age in the geologic record has been quantitatively analyzed for the Quaternary of Japan by Kiyosugi et al. (2015). This effect can be observed in Figure 8b where the curves of cumulative event number typically flatten to older ages. For instance, in the records of Glazner et al. (1999) and Kutterolf et al. (2013) 85% and 70%, respectively, of the eruptive events are concentrated within the first half of the length of the time series. In the 40 ka record of Huybers and Langmuir (2009) 80% of the events occur in the last 1000 years, i.e. in the first 1/40´s of the entire time series.

Where several cores from a given region are used to compile a tephra time series, it is essential to correlate the ash beds between cores in order to avoid multiple counting of single volcanic events. Even in single cores primary ash beds can appear to occur multiply by reworking (e.g., Eisele et al., 2015), hence distinction between primary and reworked ash beds is important. Another issue is different methods and precision of tephra age dating and the respective data density within the time series.

Sources of variations and errors include: (1) Biostratigraphic and foraminiferal $\delta^{18}O$ correlations determined at different decades may differ due to updating of methods. (2) Preservation of datable calcareous fossils may vary due to fluctuations in carbonate compensation depth (CCD). (3) Ash bed dating by linear interpolation between age tie points in cores assumes constant accumulation rate of intercalated sediments which may not be true; this risk increases the farther apart the tie points. (4) Competing age models may exist for the same drill site (e.g. Schindlbeck et al., 2018). (5) Additionally radiometric age datings of tephra beds can have variably large errors and are usually variably abundant across the entire age range (e.g., variable age resolution in lacustrine records, Kutterolf et al., 2016). (6) The density of age data throughout the time series that is variable and sometimes may not be high enough to facilitate the detection of higher frequencies.

Tephra ages derived from an age model exclusively based on sediment correlation with a global stable oxygen isotope record, which itself contains orbital tuning, carries the risk that the fitting may “artificially” transfer that tuning to the tephra record. Hence it would be better to use age models based on a combination of different dating techniques.

Drill cores on oceanic plates have changed their position over time relative to volcanic sources at subduction zones, typically moving closer to the arc. This potentially causes an increase in recorded volcanic events to the younger core sections (e.g., Kennett et al., 1977) particularly with fast plate motion such as in the Pacific.

There are two ways by which tephra time series can be described, by tephra thickness and by event number. Prueher and Rea (2001), for example, use the variation in slope of a curve of cumulative thickness over age to distinguish times of increased or reduced volcanic activity. However, in many records ash bed thicknesses are not consistently reported, volcanic eruptions of a given magnitude may be represented by variable thicknesses depending on position relative to source, ash layer thickness may be reduced by erosion, many ash beds do not have a sharply defined top but gradually change into ash-rich sediment, and cryptotephras (ash dispersed in sediment) have no thickness at all. Therefore most tephra records are described by event numbers, meaning they are binary records, where each point in time has a value of either 0 or 1 (e.g., Fig. 8a).

Methods of statistical treatment

One way to investigate binary tephra records is to analyze curves of cumulative event number over age (Fig. 8b). For example, McGuire et al. (1997) used this approach to identify divergences from a straight line in cumulative number versus age, which reflect times of increased or reduced rate in volcanism analogous to the thickness approach mentioned above. More commonly, however, the binary series is converted into a continuous series either by applying kernel methods (Newall et al., 2006) or by running a moving average over the data, whereby different time windows and progression steps have been employed (Jellinek et al., 2004; Kutterolf et al., 2013; Schindlbeck et al., 2018). These authors as well as Paterne et al. (1990) then used somewhat different techniques of spectral analysis to investigate the frequency contents of the tephra time series. While each published approach certainly had its justification and value, the diverse methods make it difficult to compare the results and may lead, at least in part, to different results (e.g., observed periodicities). Another problem is the different lengths of the records. The 23 kyr periodicity has been observed in relatively short time series (e.g., Paterne et al., 1990), but was not identified in longer records (e.g., Kutterolf et al., 2013). One cause for this may be - next to required high data and age resolution - the increasing likelihood of missing volcanic events with increasing age, which masks high frequency variations in volcanic activity at age. It can therefore neither be proven nor disproven whether a 23 kyr periodicity existed consistently over the last millions of years.

In order to improve comparability between data sets, we re-analyzed the tephra time series by the same approach. We chose records for which the individual data are available, which are to our knowledge well dated, cover a sufficient length in time, and presumably do not strongly suffer from sampling bias (Fig. 8a; Table 1). The re-analyzed records are **Jell04** with the East Californian data from Jellinek et al. (2004)

and Glazner et al. (1999), **PR01** with the northwestern Pacific data from Prueher and Rea (2001), the Pacific Ring of Fire tephra compilation **K13** from Kutterolf et al. (2013), and the Izu-Bonin-Japan tephra series **Sch18** from IODP hole U1437B recorded by Schindlbeck et al. (2018). Table 1 summarizes essential features of these records such as their different age ranges and number of events, and their cumulative number of events over time is displayed in Figure 8b.

The time series constitute binary time series equally sampled at 10 years intervals. A value of 0 indicates that no eruption took place, a value of 1 indicates an eruption. We limited longer records to the last 700 kyr; the McGuire et al. (1997) and Paterne et al. (1990) data sets only cover the last 200 kyr and are therefore not included in the following analyses despite high sample density and the presence of high-frequency periodicities. The four records extend from before and across the post-MPT period, and include multiple 100 kyr cycles.

The number of events in each record varies. The slope of the cumulative event number curves in Figure 8b is proportional to the density of the eruption record and typically deviate from a straight line, which represents a homogeneous time distribution (which means no periodicities). For all time series, short and long term deviations are visible. Particularly eye catching are the change from high to lower slope at ~100 kyr in the K13 and ~200kyr in the Jell04 time series. Overall the K13 record exhibits the largest slope due to its highest event density (450 events in 1.2 Myr). A high density is also present in the McG97 record (107 events in 180 kyr). The Sch18 time series has the lowest density (162 events in 1-1 Myr). Over the entire age range, the slope of the cumulative curves slightly decreases as an artifact of increasing under-recording of events to older ages (cf. Kiyosugi et al., 2015). On the other hand, the PR01, Sch18 and Jell04 time series show an increase in slope across the first 100-400 kyr where event density is relatively low.

In the following we do not apply a moving average to the data as it was done in the previous studies, because this acts as a low-pass filter eliminating variations with a period shorter than the moving-average time window. Instead we analyze the binary data directly, which should lead to a better comparability between the different time series. Moreover, unlike in earlier studies, we first perform the analysis in the frequency domain rather than in the time domain; we will discuss the time domain analysis in a later section.

Spectral density estimations in the frequency domain

In order to understand the behavior of binary data series in spectral analysis, we first analyze an artificial binary sequence consisting of 10 events every 100 ka and compare this to a time series consisting of a sine with a period of 100 kyr (Fig. 9a, b). We calculate the spectra using the multi-taper spectral analysis method (Percival and Walden, 1998; Thomson, 1982), which reduces the estimation bias in the power spectra. It estimates the spectral density for each frequency by obtaining multiple independent estimates from the same time series using a sequence of discrete prolate spheroidal (DPSS) tapers. The resulting spectral resolution is determined by the time-bandwidth product. A larger time-bandwidth product results in a smoother spectrum, i.e. less resolution in the frequency domain. A smaller value gives higher spectral resolution. Throughout this analysis we use a narrow time-bandwidth product of 2.0.

The resulting spectrum of the sine wave consists of a single peak at a frequency of 1/100 kyr. Due to the pulsed nature of the binary sequence, the corresponding spectrum shows a series of spikes of equal height, situated at the fundamental frequency of 1/100 kyr and at the higher harmonic frequencies at 2/100 kyr, 3/100 kyr etc. (Fig. 9b). Thus, a particular periodicity in volcanic eruptions manifests itself not by a single peak at that frequency in the spectrum but by a series of peaks with similar amplitudes at the harmonics of the fundamental frequency (Fig. 9b). This renders it more difficult to identify different periodicities in the discrete, binary volcanic records than, for example, in the more smoothly varying continuous $\delta^{18}O$ record, where only one peak is associated with a particular frequency. The spectra will be particularly difficult to interpret if more than one periodicity is present and the resulting spectral patterns superimpose and affect each other. This is shown in Figure 9c where we analyzed an artificial binary sequence consisting of 10 events every 100 ka as well as every 41 ka. Evidently the overlay of just two periodicities in the time series can generate an already fairly complex pattern of peaks in the frequency spectrum.

In a further step, Figure 10 shows the spectra of the re-analyzed natural ash and $\delta^{18}O$ time series for the last 700 kyr compared with bars which indicate the expected positions of peaks for the pure 100 kyr and 40 kyr periods derived from the artificial time series as shown in Figure 9c. As a reference we also include the spectrum of an artificial random binary sequence. The $\delta^{18}O$ time series, which is known to contain the dominant 41 and 100 kyr periodicities, has spectral density peaks at the corresponding primary frequencies indicated by the left-most blue and pink bars.

For some of the ash time series, a visually good agreement in frequency position is seen at the expected peak positions for the pure 100 kyr and 40 kyr periodicities, both for the primary (left-most) frequencies and for some of the harmonic frequencies. In contrast, no systematic correlation is seen for the spectrum of the random time series (Figure 10f). Figures 10b to 10e strongly suggest that all four ash time series contain the ~40 kyr and ~100 kyr periodicities although these have not always been found in the previous (time domain) studies (Table 1).

At first order, if an underlying global periodic physical process exists that influences eruption frequencies next to the local effects, one would expect that the tephra spectra are correlated with each other. This hypothesis is tested by calculating the mutual correlations between the different ash record spectra. Table 2a shows the correlation coefficients for correlation over a period range of 160 kyr to 10kyr. The range was chosen since it encompasses the main Milankovitch periods of 100kyr, 41kyr and 23kyr. However, due to the decreasing density of volcanic events with increasing age, we do not necessarily expect conclusive results for the 23kyr period peak. The chosen range excludes longer periods, which are more strongly influenced by long term sampling bias, and shorter periods, which may not be represented adequately due to low sampling densities. Table 2b lists the probabilities that the derived correlation coefficients may be reached by chance if the paired spectra were actually uncorrelated. The spectra of K13, Sch18 and PR01 are statistically significantly correlated, with probabilities of false correlations below <2%. The spectra correlations with the Jell04 time series mostly do not yield statistically significant correlation coefficients and higher (but still small) probabilities for a false correlation; an exception is a weak correlation with Sch18 (probability of false positive less than 4%). The observed correlation coefficients are generally not close to one because all time series contain abundant “noise” from uncorrelated frequency contents.

The lack of any statistically significant correlation between the tephra spectra and the spectrum of a random time series indicates that the analysis is statistically valid, and further verifies that correlations among the tephra spectra are significant. We can thus conclude that there is a high probability that the eruption frequency variations observed at different regions have a common underlying frequency component that point to a global underlying mechanism.

We further correlate the tephra spectra with the $\delta^{18}O$ spectrum, bearing in mind that the correlations may be biased by the existence of the harmonic peaks in the tephra spectra. However, the coefficients of correlation are similar or even better than the coefficients of correlation between the ash records (Table 2). They are again highest and statistically most significant for K13, Sch18 and PR01 records, but low for the Jell04 record. For our test case against the spectrum of a random time series the coefficients are almost zero. These results further support the hypothesis that there is a common underlying periodic mechanism that links eruption frequencies and climate.

<u>Correlations in the time domain</u>

The approach in the frequency domain offers the opportunity to identify the frequency distribution of the signal, yet it does not allow to identify the phase shift between the time series. Therefore we now attempt to correlate the tephra time series with the $\delta^{18}O$ time series such that the correlation coefficient is determined as a function of time lag. Positive lags in our definition are due to a shift of the ash record towards the past and negative lags to a shift towards the present. The correlation tests how well one record can be transformed into the other by a linear function and we expect a maximum correlation (positive or negative) for a time shift that aligns variations in the ash and $\delta^{18}O$ records.

To achieve meaningful values of the correlation coefficient, we cannot use the binary series employed in the last section because the large number of zeros in the record would result in very low correlation values. Instead, we need to create a continuous time series and hence return to applying a 10 kyr phase-stable running average to the ash record. Figure 11 shows the resulting smoothed time series in which frequency peaks are mostly distributed along the age range. Only the Jell04 (~10 ka and ~200 ka) and Sch18 (~340 ka) series contain unusually large peaks.

Figure 12 shows the correlations of these ash time series with the $\delta^{18}O$ time series as a function of lag. Also included is the correlation of a random time series (which in theory contains variations with all frequencies) with $\delta^{18}O$, which can serve as a threshold above which a correlation becomes statistically significant. The best correlation is Sch18 with $\delta^{18}O$. Sch18 attains the largest negative correlation coefficient (~-0.5) at positive phase shift of +13.2 kyr. This implies that a maximum eruption frequency occurs 13.5 ky before a minimum in $\delta^{18}O$ and 7 kyr after the glacial maximum respectively, which places it in the transition from cold to warm climate.

However, there are some critical issues of such time domain correlations. In contrast to Sch18 the correlation coefficients for K13, Jell04, and PR01 are relatively low and close to those for the random time series making it difficult to determine any phase shift; this also implies a less clear correlation with sea-level change. Since Sch18 is the only time series that is from a region completely unaffected by ice loading, it is tempting to interpret these contrasting results to reflect some different driving mechanism in glaciated and non-glaciated as well as oceanic and continental regions. Yet our analysis in the frequency domain has demonstrated that all four tephra series contain the important ~100 kyr and ~40 kyr periodicities that also dominate the $\delta^{18}O$ record, which is the generally accepted sea-level proxy. The noise from other frequencies is large in all tephra series and the $\delta^{18}O$ record, leading to correlation coefficients generally well below 1 (table 2). The dominant frequencies in $\delta^{18}O$ are not precisely defined but form broad peaks over some frequency range (e.g., the 100 kyr eccentricity does in fact range from 95 to 125 kyr), which introduces relatively large errors for the calculated time lag. Moreover, the data density of the time series poses a lower limit on the time lag that can be determined (Nowell et al., 2006). Especially more evenly distributed and more precise high-resolution ages of the tephra time series may also provide solutions for some of the above described variations and problems. As a consequence, it remains difficult to judge whether or not the periodicities in eruption frequency occur synchronously between the records, and the precise relationshipwith the $\delta^{18}O$ record. In summary, we conclude that the correlation in the time domain suffers from a number of uncertainties, which make it difficult to interpret the results. The results of analysis in the frequency domain, however, show that significant correlations exist even though correlation coefficients in the time domain remain near the level for the random series.

Conclusions

The four re-analyzed tephra records cover a wide range in geographic latitudes and include oceanic and continental settings, as well as glaciated and non-glaciated regions. Three records represent from regional volcanic sources, and one record is a semi-global compilation. Yet our analysis of the data in the frequency domain demonstrated that all contain the ~40 kyr and ~100 kyr periodicities that also dominate the $\delta^{18}O$ spectrum. The frequency spectra of the tephra and $\delta^{18}O$ records are significantly correlated. This observation supports the hypothesis that orbital-driven global climate changes interact with the volcanic eruption frequency regionally and globally.

In order to investigate the relative timing or synchronicity of volcanic and climate events, analysis in the time domain needs to be performed as was done in previous studies (Jellinek et al., 2004; Nowell et al., 2006; Kutterolf et al., 2013). However, the simultaneous analysis of the four best-characterized tephra records shows that correlations suffer from a number of uncertainties and results should be used with caution. For example, Jellinek et al. (2004) determined different time lags when correlating silicic (3.2±4.2 kyr) and basaltic (11.2±2.3 kyr) tephra records separately with the SPECMAP climate record (in fact, they correlated the first derivatives). But are these different time lags the results of different physical processes or of the different nature of the two data sets? Jellinek et al. (2004), Nowell et al. (2006), Kutterolf et al. (2013) and Schindlbeck et al. (2018) consistently obtained time lags that place the peak in volcanism in the deglaciation period. The observations from Iceland and Alaska for volcanism since the last glacial maximum (Fig. 3) combined with physical modeling results (e.g., Jull and McKenzie, 1996; Schmidt et al., 2013; Albino et al., 2010) support such timing as plausible. However, considering the uncertainties discussed above, can the time lags really be determined with such precision to hit the deglaciation periods which typically last about 20 kyr for the 100 kyr cycles and are much shorter for the 41 kyr cycles? Moreover, most volcanoes that contributed to the K13 and Sch18 tephra records lie well outside glaciated regions. Is it plausible that volcanism increases at low latitudes where the rising sea-level increases the lithospheric pressure while at the same time high latitude volcanism increases presumably as consequence of the decreasing lithospheric load as glaciers melt?

Most likely volcanic reactions to global climate changes are modulated by geotectonic setting, regional geologic conditions, and geographic position but with the presently available abundance and quality of the tephra and age records and the associated uncertainties in the time domain analyses it is not yet possible to disentangle these various influences. Therefore more precise tephra time series (preservation and age optimized) from different regions (glaciated versus non-glaciated) and geological settings (island arcs, continental arcs, intraplate) are needed together with standardized statistical analysis to decipher the impact of these factors on a global perspective of how climate may control volcanism. Disentangling these influences will also provide better understanding of the physical processes that regulate the feedback between global and regional volcanism and climate changes.

Acknowledgements

We would like to thank all colleagues that have been involved in creating the basic literature for this review paper for doing a great job and keeping this topic running for the last decades. We hope that this review encourages more work on precise tephra time series needed to extend the statistical treatment to unravel the mystery of both, the cyclicity in volcanic records and the coincidence with climate proxies. SK and JCS want to thank the German Research Foundation (SCHI1349/1-1, KU2685/2-1, 2-2, 4-1) as well as IODP for providing support. In particular we also want to thank two anonymous reviewers for their helpful comments and suggestions, which helped to improve this paper.

References:

Albino, F., Pinel, V. and Sigmundsson, F., 2010. Influence of surface load variations on eruption likelihood: application to two Icelandic subglacial volcanoes, Grímsvötn and Katla. Geophysical Journal International, 181(3): 1510-1524.

Bond, D.P. and Wignall, P.B., 2014. Large igneous provinces and mass extinctions: an update. Volcanism, Impacts, and Mass Extinctions: Causes and Effects, 505. Geological Society of America Special Papers.

Bredemeyer, S. and Hansteen, T.H., 2014. Synchronous degassing patterns of the neighbouring volcanoes Llaima and Villarrica in south-central Chile: the influence of tidal forces. International Journal of Earth Sciences, 103(7): 1999-2012.

Briffa, K.R., Osborn, T.J. and Schweingruber, F.H., 2004. Large-scale temperature inferences from tree rings: a review. Global and Planetary Change, 40(1): 11-26.

Cadet, J.-P., Pouclet, A., Thisse, Y., Bardintzeff, J.M. and Azéma, J., 1982a. Middle America Neogene explosive volcanism and ash layers: evidence from the Middle America Trench transect, Deep Sea Drilling Project 67. In: J. Aubouin, R. von Huene and e. al. (Editors), Init. Repts. DSDP. U.S. Govt. Printing Office, Washington, pp. 475-491.

Cadet, J.-P., Thisse, Y., Pouclet, A., Bardintzeff, J.M. and Stephan, J.F., 1982b. Tephra from Deep Sea Drilling Project Leg 66: Middle American Trench

Transect (Southern Mexico). In: J.S. Watkins, J.C. Moore and e. al. (Editors), Init. Repts. DSDP. U.S. Govt. Printing office, Washington, pp. 687-698.
Cambray, H., Pubellier, M., Jolivet, L. and Pouclet, A., 1995. Volcanic activity recorded in deep-sea sediments and the geodynamic evolution of western Pacific island arcs. In: B. Taylor and J. Natland (Editors), Active Margins and Marginal Basins of the western Pacific. Geophysical Monograph, American Geophysical Union, Washington, pp. 97-124.
Cambray, H. and Cadet, J., 1994. Testing global synchronism in peri-Pacific arc volcanism. Journal of Volcanology and Geothermal Research, 63(3-4): 145-164.
Campbell, I.H., Czamanske, G.K., Fedorenko, V.A., Hill, R.I. and Stepanov, V., 1992. Synchronism of the Siberian Traps and the Permian-Triassic Boundary. Science, 258: 1760-1763.
Carey, S. and Sigurdsson, H., 2000. Grain size of Miocene volcanic ash layers from Sites 998, 999, and 1000: Implications for source areas and dispersal. In: R.M. Leckie, H. Sigurdsson, G.D. Acton and G. Draper (Editors), Proceedings ODP, Scientific Results 165, pp. 101-110.
Costa, K.M., McManus, J.F., Middleton, J.L., Langmuir, C.H., Huybers, P.J., Winckler, G. and Mukhopadhyay, S., 2017. Hydrothermal deposition on the Juan de Fuca Ridge over multiple glacial–interglacial cycles. Earth and Planetary Science Letters, 479: 120-132.
Courtillot, V.E. and Renne, P.R., 2003. On the ages of flood basalt events. Comptes Rendus Geoscience, 335(1): 113-140.
Cronin, T.M., 2012. Rapid sea-level rise. Quaternary Science Reviews, 56: 11-30.
Crowley, J.W., Katz, R.F., Huybers, P., Langmuir, C.H. and Park, S.-H., 2015. Glacial cycles drive variations in the production of oceanic crust. Science, 347(6227): 1237-1240.
Deligne, N.I., Coles, S.G. and Sparks, R.S.J., 2010. Recurrence rates of large explosive volcanic eruptions. Journal of Geophysical Research, 115: doi: 10.1029/2009JB006554
Dzurisin, D., 1980. Influence of fortnightly Earth tides at Kilauea Volcano, Hawaii. Geophysical Research Letters, 7(11): 925-928.
Eisele, S., Freundt, A., Kutterolf, S., Ramalho, R.S., Kwasnitschka, T., Wang, K.L., Hemming, S.R., 2015. Stratigraphy of the Pleistocene, phonolitic Cão Grande Formation on Santo Antão, Cape Verde. Journal of Volcanology and Geothermal Research, 301: 204-220.
Glazner, A.F., Manley, C.R., Marron, J.S. and Rojstaczer, S., 1999. Fire or ice: anticorrelation of volcanism and glaciation in California over the past 800,000 years. Geophysical Research Letters, 26: 1759-1762.
Hein, J.R., Scholl, D.W. and Miller, J., 1978. Episodes of Aleutian Ridge explosive volcanism. Science, 199: 137-141.
Highwood, E.J. and Stevenson, D.S., 2003. Atmospheric impact of the 1783-1784 Laki eruption: Part II Climatic effect of sulphate aerosol. Atmospheric Chemistry and Physics, 3: 1177-1189.
Hofmann, C., Courtillot, V., Féraud, G., Rochette, P., Yirgu, G., Ketefo, E. and Pik, R., 1997. Timing of the Ethiopian flood basalt event and implications for plume birth and global change. Nature, 389: 838.
Huybers, P. and Langmuir, C., 2009. Feedback between deglaciation, volcanism, and atmospheric CO_2. Earth and Planetary Science Letters, 286(3): 479-491.

Jellinek, A.M., Manga, M. and Saar, M.O., 2004. Did melting glaciers cause volcanic eruptions in eastern California? Probing the mechanics of dike formation. Journal of Geophysical Research, 109: doi: 10.1029/2004JB002978.
Johnston, M.J.S. and Mauk, F.J., 1972. Earth Tides and the Triggering of Eruptions from Mt Stromboli, Italy. Nature, 239: 266.
Jull, M. and McKenzie, D., 1996. The effect of deglaciation on mantle melting beneath Iceland. Journal of Geophysical Research: Solid Earth, 101(B10): 21815-21828.
Jupp, T.E., Pyle, D.M., Mason, B.G. and Dade, W.B., 2004. A statistical model for the timing of earthquakes and volcanic eruptions influenced by periodic processes. Journal of Geophysical Research: Solid Earth, 109(B2). doi:10.1029/2003JB002584
Kasahara, J. and Sato, T., 2001. Tidal Effects on Volcanic Earthquakes and Deep-sea Hydrothermal Activity Revealed by Ocean Bottom Seismometer Measurements. Journal of the Geodetic Society of Japan, 47(1): 424-433.
Kennett, J.P., McBirney, A.R. and Thunell, R.C., 1977. Episodes of Cenozoic volcanism in the circum-Pacific region. Journal of Volcanology and Geothemal Research, 2: 145-163.
Kennett, J.P. and Thunell, R.C., 1975. Global increase in Quaternary explosive volcanism. Science, 187(4176): 497-502.
Kiyosugi, K., Connor, C., Sparks, R.S.J., Crosweller, H.S., Brown, S.K., Siebert, L., Wang, T. and Takarada, S., 2015. How many explosive eruptions are missing from the geologic record? Analysis of the quaternary record of large magnitude explosive eruptions in Japan. Journal of Applied Volcanology, 4(1): 17. doi: 10.1186/s13617-015-0035-9
Kutterolf, S., Jegen, M., Mitrovica, J.X., Kwasnitschka, T., Freundt, A. and Huybers, P., 2013. A detection of Milankovitch frequencies in global volcanic activity. Geology, 41(2): 227-230.
Kutterolf S., Schindlbeck, J.C., Anselmetti, F.S., Ariztegui, D., Brenner, M., Curtis, J.H., Schmidt, D., Hodell, D.A., Müller, A.D., Peréz, L., Peréz, W., Schwalb, A., Frische, M., Wang, K-L. (2016) A 400-ka tephrochronological framework for Central America from Lake Petén Itzá (Guatemala) sediments, Quart Sci Rev., 150, 200-220, doi:10.1016/j.quascirev.2016.08.023
Lambeck, K., Rouby, H., Purcell, A., Sun, Y. and Sambridge, M., 2014. Sea level and global ice volumes from the Last Glacial Maximum to the Holocene. Proceedings of the National Academy of Sciences, 111: 15296-15303.
Lavigne, F., Degeai, J.-P., Komorowski, J.-C., Guillet, S., Robert, V., Lahitte, P., Oppenheimer, C., Stoffel, M., Vidal, C.M., Surono, Pratomo, I., Wassmer, P., Hajdas, I., Hadmoko, D.S. and de Belizal, E., 2013. Source of the great A.D. 1257 mystery eruption unveiled, Samalas volcano, Rinjani Volcanic Complex, Indonesia. Proceedings of the National Academy of Sciences, 110(42): 16742; doi: 10.1073/pnas.1307520110
Lewis, S.E., Sloss, C.R., Murray-Wallace, C.V., Woodroffe, C.D. and Smithers, S.G., 2013. Post-glacial sea-level changes around the Australian margin: a review. Quaternary Science Reviews, 74: 115-138.
Lisiecki, L.E. and Raymo, M.E., 2005. A Pliocene-Pleistocene stack of 57 globally distributed benthic d18O records. Paleoceanography, 20(PA1003): doi:10.1029/2004PA001071.
Lund, D.C. and Asimow, P.D., 2011. Does sea level influence mid-ocean ridge magmatism on Milankovitch timescales? Geochemistry, Geophysics, Geosystems, 12(12): doi:10.1029/2011GC003693.

Lund, D.C., Asimow, P.D., Farley, K.A., Rooney, T.O., Seeley, E., Jackson, E.W. and Durham, Z.M., 2016. Enhanced East Pacific Rise hydrothermal activity during the last two glacial terminations. Science, 351(6272): 478-482.

MacLennan, J., Jull, M., McKenzie, D., Slater, L. and Grönvold, K., 2002. The link between volcanism and deglaciation in Iceland. Geochemistry, Geophysics, Geosystems, 3(11): doi: 10.1029/2001GC000282.

Mahony, S.H., Sparks, R.S.J., Wallace, L.M., Engwell, S.L., Scourse, E.M., Barnard, N.H., Kandlbauer, J. and Brown, S.K., 2016. Increased rates of large-magnitude explosive eruptions in Japan in the late Neogene and Quaternary. Geochemistry, Geophysics, Geosystems, 17(7): 2467-2479.

Manning, J.G., Ludlow, F., Stine, A.R., Boos, W.R., Sigl, M. and Marlon, J.R., 2017. Volcanic suppression of Nile summer flooding triggers revolt and constrains interstate conflict in ancient Egypt. Nature Communications, 8(1): 900; doi: 10.1038/s41467-017-00957-y

Mason, B.G., Pyle, D.M., Dade, W.B. and Jupp, T., 2004. Seasonality of volcanic eruptions. Journal of Geophysical Research: Solid Earth, 109(B4). doi:10.1029/2002JB002293

McCormick, M.P., Thomason, L.W. and Trepte, C.R., 1995. Atmospheric effects of the Mt. Pinatubo eruption. Nature, 373: 399-404.

McGuire, W.J., Howarth, R.J., Firth, C.R., Solow, A.R., Pullen, A.D., Saunders, S.J., Stewart, I.S. and Vita-Finzi, C., 1997. Correlation between rate of sea-level change and frequency of explosive volcanism in the Mediterranean. Nature, 389: 473-476.

McLean, D.M., 1985. Deccan traps mantle degassing in the terminal Cretaceous marine extinctions. Cretaceous Research, 6(3): 235-259.

McNutt, S.R. and Beavan, R.J., 1987. Eruptions of Pavlof Volcano and their possible modulation by ocean load and tectonic stresses. Journal of Geophysical Research: Solid Earth, 92(B11): 11509-11523.

Middleton, J.L., Langmuir, C.H., Mukhopadhyay, S., McManus, J.F. and Mitrovica, J.X., 2016. Hydrothermal iron flux variability following rapid sea level changes. Geophysical Research Letters, 43(8): 3848-3856.

Miller, G.H., Geirsdóttir, Á., Zhong, Y., Larsen, D.J., Otto-Bliesner, B.L., Holland, M.M., Bailey, D.A., Refsnider, K.A., Lehman, S.J., Southon, J.R., Anderson, C., Björnsson, H. and Thordarson, T., 2012. Abrupt onset of the Little Ice Age triggered by volcanism and sustained by sea-ice/ocean feedbacks. Geophysical Research Letters, 39(2): doi: 10.1029/2011GL050168.

Mudelsee, M. & Schulz, M., 1997. The Mid-Pleistocene climate transition: onset of 100 ka cycle lags ice volume build-up by 280 ka. Earth Planet. Sci. Lett. 151, 117–123.

Nowell, D.A.G., Jones, M.C. and Pyle, D.M., 2006. Episodic Quaternary volcanism in France and Germany. Journal of Quaternary Science, 21(6): 645-675. doi:10.1002/jqs.1005

Oppenheimer, C. (2003). Climatic, environmental and human consequences of the largest known historic eruption: Tambora volcano (Indonesia) 1815. Progress in Physical Geography: Earth and Environment, 27(2), 230–259. https://doi.org/10.1191/0309133303pp379ra.

Pagli, C. and Sigmundsson, F., 2008. Will present day glacier retreat increase volcanic activity? Stress induced by recent glacier retreat and its effect on magmatism at the Vatnajökull ice cap, Iceland. Geophysical Research Letters, 35(9):doi: 10.1029/2008GL033510.

Patanè, G., Montalto, A., Imposa, S. and Menza, S., 1994. The role of regional tectonics, magma pressure and gravitational spreading in earthquakes of the eastern sector of Mt. Etna volcano (Italy). Journal of Volcanology and Geothermal Research, 61(3): 253-266.
Paterne, M., Labeyrie, J., Guichard, F., Mazaud, A. and Maitre, F., 1990. Fluctuations of the Campanian explosive volcanic activity (South Italy) during the past 190,000 years, as determined by marine tephrochronology. Earth and Planetary Science Letters, 98(2): 166-174.
Percival, D.B., Walden, A.T., 1998. Spectral Analysis for Physical Applications: Multitaper and Conventional Univariate Techniques 2nd ed.; Cambridge University Press, Cambridge.
Praetorius, S., Mix, A., Jensen, B., Froese, D., Milne, G., Wolhowe, M., Addison, J. and Prahl, F., 2016. Interaction between climate, volcanism, and isostatic rebound in Southeast Alaska during the last deglaciation. Earth and Planetary Science Letters, 452: 79-89.
Prueher, L.M., Rea, D.K., 1998. Rapid onset of glacial conditions in the subarctic North Pacific region at 2.67 Ma: clues to causality. Geology 26, 1027-1030.
Prueher, L.M. and Rea, D.K., 2001. Tephrachronology of the Kamchatka - Kurile and Aleutian arcs: evidence for volcanic episodicity. Journal of Volcanology and Geothermal Research, 106: 67-84.
Pyle, D.M., 1995. Mass and energy budgets of explosive volcanic eruptions. Geophysical Research Letters, 22(5): 563-566.
Railsback, L.B., Gibbard, P.L., Head, M.J., Voarintsoa, N.R.G., and Toucanne, S., 2015. An optimized scheme of lettered marine isotope substages for the last 1.0 million years, and the climatostratigraphic nature of isotope stages and substages. Quaternary Science Reviews 111, 94-106.
Rampino, M.R., Self, S., and Fairbridge, R.W., 1979. Can rapid climatic change cause volcanic eruptions?: Science, v. 206, p. 826–829.
Rampino, M.R. and Self, S., 1982. Historic eruptions of Tambora (1815), Krakatau (1883), and Agung (1963), their stratospheric aerosols, and climate impact. Quaternary Research, 18: 127-143.
Rampino, M.R. and Self, S., 1993. Climate-Volcanism Feedback and the Toba Eruption of ~74,000 Years Ago. Quaternary Research, 40(3): 269-280.
Rawson, H., Pyle, D.M., Mather, T.A., Smith, V.C., Fontijn, K., Lachowycz, S.M. and Naranjo, J.A., 2016. The magmatic and eruptive response of arc volcanoes to deglaciation: Insights from southern Chile. Geology, 44(4): 251-254.
Robock, A., 2000. Volcanic eruptions and climate. Reviews of Geophysics, 38: 191-219.
Robock, A., 2002a. The Climatic Aftermath. Science, 295: 1242-1244.
Robock, A., 2002b. Pinatubo eruption: The climatic aftermath. Science, 295: 1242-1244.
Ryan, W.B.F., Carbotte, S.M., Coplan, J.O., O'Hara, S., Melkonian, A., Arko, R., Weissel, R.A., Ferrini, V., Goodwillie, A., Nitsche, F., Bonczkowski, J. and Zemsky, R., 2009. Global Multi-Resolution Topography synthesis. Geochemistry, Geophysics, Geosystems, 10(3): Q03014.
Scharff, L., Hort, M. and Varley, N.R., 2015. Pulsed Vulcanian explosions: A characterization of eruption dynamics using Doppler radar. Geology, 43(11): 995-998.
Schindlbeck, J.C., Kutterolf, S., Freundt, A., Straub, S.M., Wang, K.-L., Jegen, M., Hemming, S.R., Baxter, A.T. and Sandoval, M.I., 2015. The Miocene Galápagos ash layer record of Integrated Ocean Drilling Program Legs 334 and

344: Ocean-island explosive volcanism during plume-ridge interaction. Geology, 43(7): 599-602.

Schindlbeck, J.C., Jegen, M., Freundt, A., Kutterolf, S., Straub, S.M., Mleneck-Vautravers, M.J., McManus, J., 100- kyr cyclicity in volcanic ash emplacement: evidence from a 1.1 Myr tephra record from the NW Pacific, Scientific Reports, doi:10.1038/s41598-018-22595-0

Schmincke, H.-U., 2004. Volcanism. Springer-Verlag Berlin Heidelberg, 324 pp.

Schmidt, P., Lund, B., Hieronymus, C., Maclennan, J., Árnadóttir, T. and Pagli, C., 2013. Effects of present-day deglaciation in Iceland on mantle melt production rates. Journal of Geophysical Research: Solid Earth, 118(7): 3366-3379.

Shackleton, N.J., 1987. Oxygen isotopes, ice volume and sea level. Quaternary Science Reviews, 6(3): 183-190.

Shane, P., Froggatt, P., Black, T. and Westgate, J.A., 1995. Chronology of Pliocene and Quaternary bioevents and climatic events from fission-track ages on tephra beds, Wairarapa, New Zealand. Earth and Planetary Science Letters, 130: 1241-1254.

Sigl, M., Winstrup, M., McConnell, J.R., Welten, K.C., Plunkett, G., Ludlow, F., Büntgen, U., Caffee, M., Chellman, N., Dahl-Jensen, D., Fischer, H., Kipfstuhl, S., Kostick, C., Maselli, O.J., Mekhaldi, F., Mulvaney, R., Muscheler, R., Pasteris, D.R., Pilcher, J.R., Salzer, M., Schüpbach, S., Steffensen, J.P., Vinther, B.M. and Woodruff, T.E., 2015. Timing and climate forcing of volcanic eruptions for the past 2,500 years. Nature, 523: 543.

Sigurdsson, H., Kelley, S., Leckie, R., Carey, S., Bralower, T. and King, J., 2000. History of circum-Caribbean explosive volcanism: 40Ar/39Ar dating of tephra layers. In: R. Leckie, H. Sigurdsson, G.D. Acton and G. Draper (Editors), Proceedings of the Ocean Drilling Program, Scientific results. Ocean Drilling Program, Scientific results, College Station, Texas, pp. 299-314.

Sigvaldason, G.E., Annertz, K. and Nilsson, M., 1992. Effect of glacier loading/deloading on volcanism: postglacial volcanic production rate of the Dyngjufjöll area, central Iceland. Bulletin of Volcanology, 54(5): 385-392.

Sottili, G., Martino, S., Palladino, D.M., Paciello, A. and Bozzano, F., 2007. Effects of tidal stresses on volcanic activity at Mount Etna, Italy. Geophysical Research Letters, 34(1): doi:10.1029/2006GL028190.

Sternai, P., Caricchi, L., Castelltort, S. and Champagnac, J.-D., 2016. Deglaciation and glacial erosion: A joint control on magma productivity by continental unloading. Geophysical Research Letters, 43(4): 1632-1641.

Sternai, P., Caricchi, L., Garcia-Castellanos, D., Jolivet, L., Sheldrake, T.E. and Castelltort, S., 2017. Magmatic pulse driven by sea-level changes associated with the Messinian salinity crisis. Nature Geoscience, 10: 783. doi:10.1038/ngeo3032

Stewart, I.S. 2017. Did sea-level change cause the switch from fissure-type to central-type volcanism at Mount Etna, Sicily? Episodes, 41 (1):7-16. doi: 10.18814/epiiugs/2018/v41i1/018002

Sumita, M. and Schmincke, H.-U., 2013. Impact of volcanism on the evolution of Lake Van I: evolution of explosive volcanism of Nemrut Volcano (eastern Anatolia) during the past> 400,000 years. Bulletin of volcanology, 75(5): 714.

Thomson, D.J., Proceedings of the IEEE 70, 1055 (1982).

Tolstoy, M., 2015. Mid-ocean ridge eruptions as a climate valve. Geophysical Research Letters, 42(5): 1346-1351.

Tuffen, H., 2010. How will melting of ice affect volcanic hazards in the twenty-first century? Philosophical Transactions of the Royal Society A:

Mathematical, Physical and Engineering Sciences, 368: 2535-2558.
Watt, S.F.L., Pyle, D.M. and Mather, T.A., 2013. The volcanic response to deglaciation: Evidence from glaciated arcs and a reassessment of global eruption records. Earth Science Reviews, 122: 77-102.

Figure captions:

Figure 1: A) Land-surface temperature variations of the last 600 years at >20°N with extreme negative excursions labeled by calendar year. Comparison with the record of volcanic eruptions (green arrows scaled by Volcanic Explosivity Index VEI) shows that volcanic eruptions are often immediately followed by negative excursions . Modified after Briffa et al. (2004). Question marks indicate uncertain eruption dates. B) Co-variation of lobal volcanic aerosol forcing and Northern Hemisphere temperature variations for the past 2,500 years after Sigl et al. (2015). Upper panel shows record of tree growth anomalies emphasizing the 40 coldest years and the 12 coldest decades. Lower panel shows the global volcanic aerosol forcing reconstructed from composite bipolar ice-core sulfate records .

Figure 2: Global topographic map (http://www.geomapapp.org; GMRT-Global Multi-Resolution Topography; Ryan et al., 2009) showing regions of major volcanic centers (red triangles) and areas where longer tephrostratigraphic records have been obtained (white boxes). Numbers in the boxes refer to the studies listed in Table 1.

Figure 3: A) Ice-volume equivalent sea level variation of the last glacial cycle (35 ka - Recent) with its 95% confidence range (gray). Major events in this interval are the Last Glacial Maximum (LGM), the Bølling-Allerød warm period (orange bar) which contains the short period of the major meltwater pulse MWP1a, and the subsequent period of peak post-glacial rebound in Iceland (gray bar; from MacLennan et al., 2002). Associated major peaks in volcanic eruptive activity at Iceland (Sigvaldason et

al., 1992), Southern Chile (Rawson et al., 2016), Southeast Alaska (Praetorius et al., 2016), and globally (Huybers and Langmuir 2009) shown as time ranges at top. Also shown is the interval of increased hydrothermal activity at mid ocean ridges (Lund et al., 2016). B) The steep postglacial increase in cumulative tephra volume from Mocho-Choshuenco volcano (Chile) after Rawson et al. (2016) (gray curve; thick lines representing mean ages and dashed lines the respective 1σ uncertainties) and the period of high eruption rates of Krafla volcanic center (light green curve) after MacLennan et al. (2002) overlap each other as well as the period of peak post-glacial rebound observed in Iceland. C) Vertical land motion due to glacial rebound in Alaska (green curve) compared with the abundance of tephra in marine sediment cores off southeast Alaska, modified after Praetorius et al. (2016). Increased tephra input into the sediments (tephra grains >125µm, red) follows the peak glacial rebound as well as the melt water pulse 1a (dashed red lines). D) The increase in global eruption rate (normalized to the last 2 ka) during the last deglaciation (purple) after Huybers and Langmuir (2009), appears to follow high rates of sea level rise (blue curve) as well as the melt water pulse 1a.

Figure 4: Upper panel: Tephra frequency over the last 5 Ma in northwestern Pacific drill cores after Prueher and Rea (2001); histogram is a 3-point moving average after binning into 100 kyr slots. Increased volcanic activity occurs ~3.1 to 2.9 Ma, 2.6 to 2.1 Ma, 1.8 to 1.4 Ma, and 0.85 to 0.1 Ma. Lower panel: Comparison of periods of increased volcanic activity observed around the Pacific Ocean by Hein et al. (1978)[1], Shane et al. (1995)[2], Kennett et al. (1975)[3], Cambray and Cadet (1994)[4], Kennett et al. (1977)[5], and Carey and Sigurdsson (2000)[6].

Figure 5: Bottom: Variations in the Campanian eruption frequency (Italy) using an 8-kyr sliding window width (pink) from Paterne et al. (1990). Gray bars indicate periods of increased Mediterranean volcanism according to McGuire et al. (1997). Top: The global $\delta^{18}O$ stack of Lisiecki and Raymo (2005) shown for comparison; low $\delta^{18}O$ values indicate warm periods with high sea level, high $\delta^{18}O$ values cold periods with low sea level (note inverted axis).

Figure 6: Top: Global $\delta^{18}O$ stacked curve (blue) of Lisiecki and Raymo (2005) for the last 1.1 Myr, identifying warm and cold periods. MPT= Mid-Pleistocene Transition, the time interval during which the $\delta^{18}O$ record changes from dominating ~40 kyr Milankovitch periods to the dominance of the ~100 kyr cycle. Center: Variation in the volcanic eruption frequency at the Izu Bonin Mariana arc (IBM, red, after Schindlbeck et al., 2018), using 10 kyr binning. Bottom: the Ring of Fire (ROF) variation in eruption frequency (green, after Kutterolf et al. 2013) using 1 kyr binning. The purple curve shows eruption frequencies for California after Glazner et al. (1999). Vertical gray bars mark marine isotope stages (MIS) after Railsback et al. (2015) for comparison.

Figure 7: a) and b) Power spectra for the silicic (green line) and basaltic (red line) time series of Californian volcanism as well as for the SPECMAP $\delta^{18}O$ reference curve for climate (dashed line) shown as a function of 0.5 kyr (a) and 1 kyr (b) bin widths after Jellinek et al. (2004). c) Comparison of the spectral density of the $\delta^{18}O$ time series after Lisecki and Raymo (2005) (blue curve) and d) the Hole U1437B ash time series (purple curve) after Schindlbeck et al. (2018). Solid lines show results post-MPT (<0.7 Ma), dashed lines syn-MPT (0.7-1.1 Ma). Dotted vertical lines mark the ranges of the characteristic 23, 41, 100 kyr Milankovitch periods. Each spectrum

has been calculated using multitaper power spectral density estimate with a time-bandwidth 3. e) Power spectrum (red solid line; computed with a time bandwidth of 1.5) with 95% confidence limits (light red field) of the ROF time series after Kutterolf et al. (2013); all values are normalized to the maximum power at the 40 kyr period.

Figure 8: A) Tephra records shown as binary bar codes from the Central Mediterranean (Paterne et al., 1990), East California (Jellinek et al., 2004; Glazner et al., 1999), the northwestern Pacific (Prueher and Rea, 2001), the Pacific Ring of Fire (Kutterolf et al., 2013), and IODP Hole U1437B of the Izu-Bonin-Japan region (Schindlbeck et al., 2018). B) Cumulative number of tephras versus age for each tephra series in A).

Figure 9: A) Artificial time series for a 100 kyr period. Vertical black lines are the binary series with 10 events every 100 kyr, red line is a continuous sine function with 100 kyr periodicity. B) Normalized power spectral density of the artificial time series in A showing the main peak at the 1/100 kyr frequency for the continuous function (red) while the binary series also shows the corresponding harmonic frequencies (1/50 kyr, 1/33 kyr, 1/25kyr … etc). C) Normalized power spectral density of an artificial binary series composed of the 100 kyr and 40 kyr periodicities (black line). Underlying bars show the expected positions of the 100 kyr (purple) and 40 kyr (blue) primary (left-most) and harmonic spectral peaks. A binary series containing just two frequencies can already generate a complex spectral pattern.

Figure 10: Normalized power spectra of (A) the $\delta^{18}O$ global stack of Lisiecki and Raymo (2005) and of the binary ash time series (B – E) discussed in the text, as well

as of a random time series (F). Pink and blue bars indicate the expected peak positions for the 100 kyr and 40 kyr periods as in Fig. 9c.

Figure 11: Variation of the number of eruptions per 10 kyr over the last 700 ka for the four investigated time series (**Jell04, PR01, K13, Sch18)** and a random time series, smoothed by applying a moving average with a 10 kyr time window. Vertical gray bars mark marine isotope stages (MIS) for comparison.

Figure 12: Correlation coefficients as a function of time lag for the correlations of the four 10kyr-filtered tephra series (**Jell04, PR01, K13, Sch18)** and the random time series with the $\delta^{18}O$ global stack after Lisiecki and Raymo (2005). The correlation is best where maximum positive (correlated) or negative (anti-correlated) coefficients are reached, and this defines the lag time.

Table 1: Comparison of major parameters of selected studies on episodic and periodic volcanic activity. Entries are sorted by length of record. Numbers in column 4 refer to geographic position in Figure 2. Colors group records according to geological settings.

Table 2: a) Correlation coefficients between the tephra time series spectra and a random time series spectrum. b) Probabilities of coincidental correlations between the time series; values <0.05 indicate statistically significant correlation.

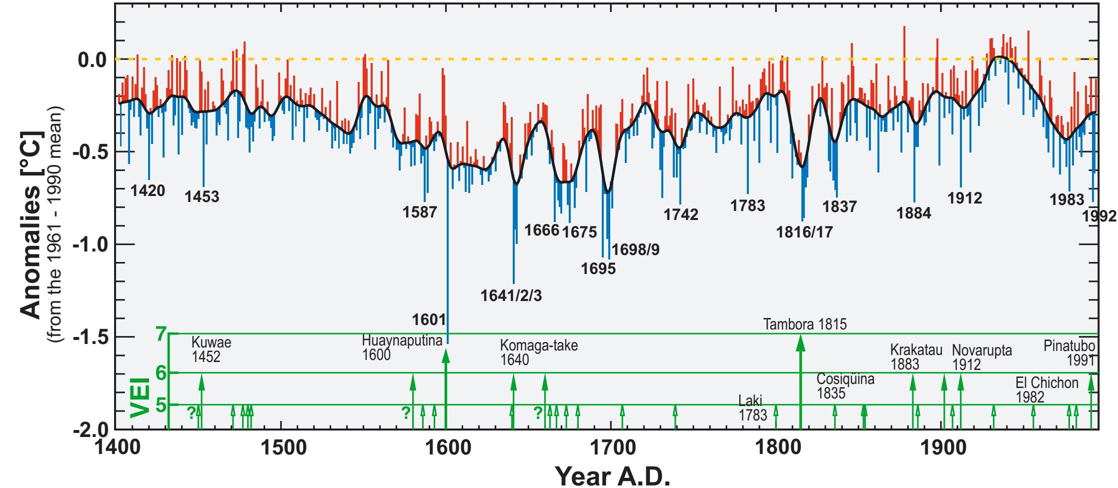

Anomalies [°C]
(from the 1961 - 1990 mean)
0.0
-0.5
-1.0
-1.5
-2.0
1420
1453
1587
1601
1641/2/3
1666
1675
1695
1698/9
1742
1783
1816/17
1837
1884
1912
1983
1992
VEI
7
6
5
?
Kuwae
1452
Huaynaputina
1600
Komaga-take
1640
Tambora 1815
Laki
1783
Cosiquina
1835
Krakatau
1883
Novarupta
1912
El Chichon
1982
Pinatubo
1991
1400
1500
1600
1700
1800
1900
Year A.D.

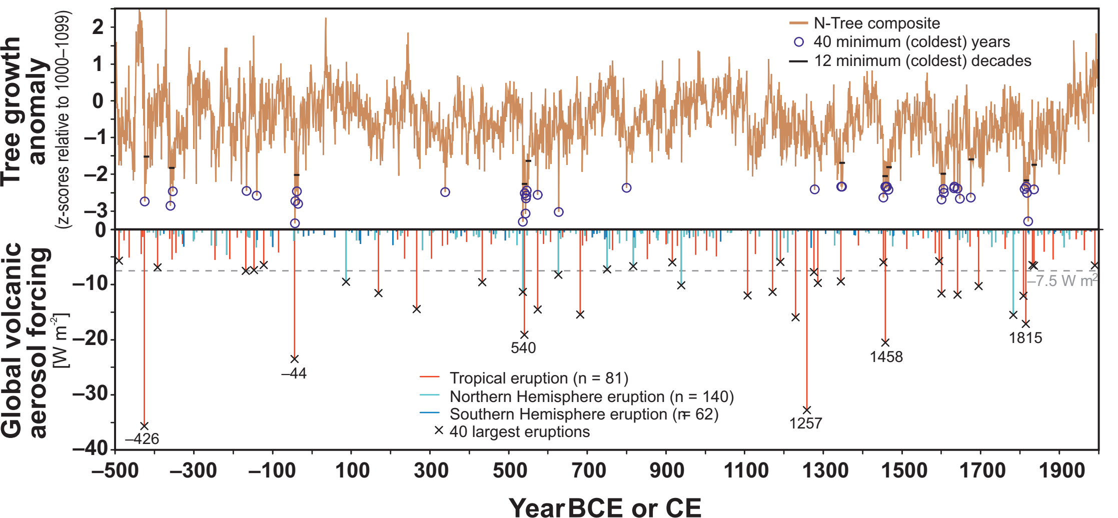

Tree growth anomaly
(z-scores relative to 1000–1099)
N-Tree composite
40 minimum (coldest) years
12 minimum (coldest) decades
Global volcanic aerosol forcing
[W m-2]
–7.5 W m-2
–426
–44
540
1257
1458
1815
Tropical eruption (n = 81)
Northern Hemisphere eruption (n = 140)
Southern Hemisphere eruption (n = 62)
40 largest eruptions
–500
–300
–100
100
300
500
700
900
1100
1300
1500
1700
1900
Year BCE or CE

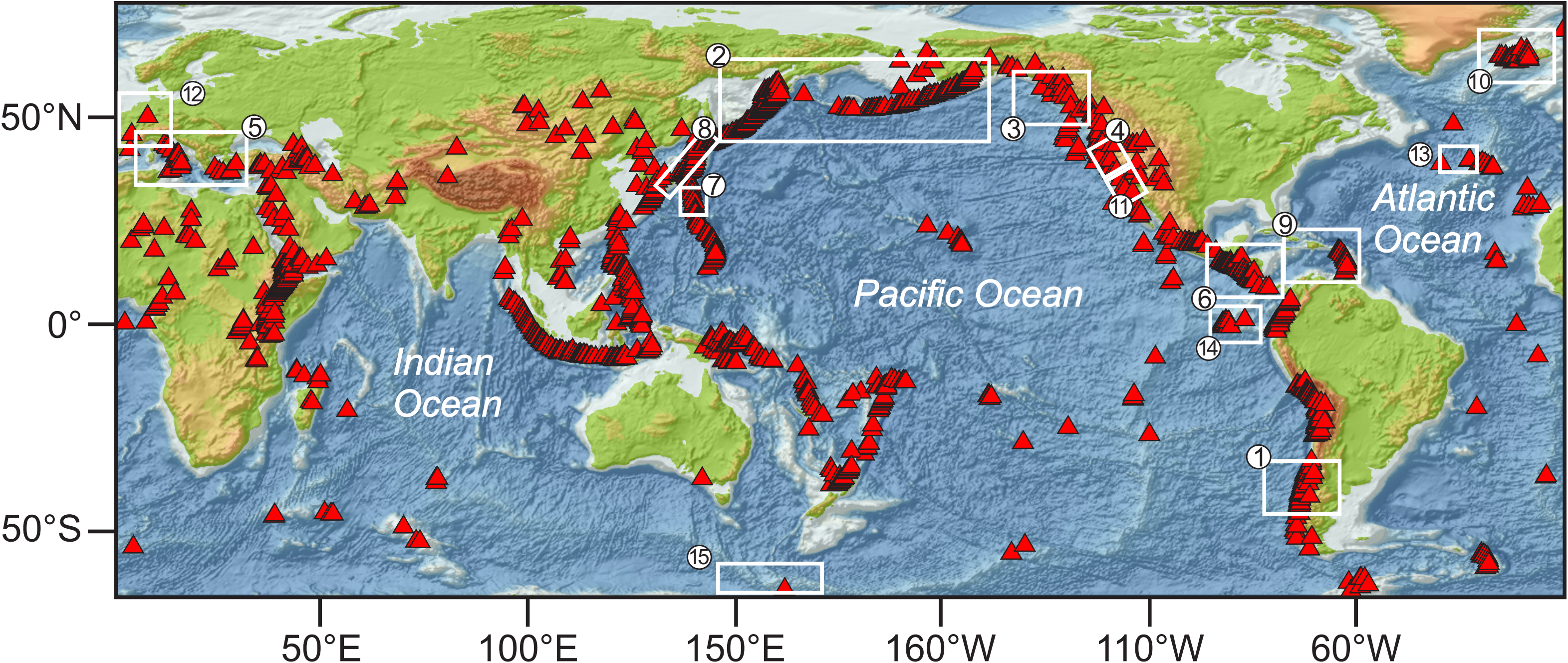
50°N
0°
50°S
50°E
100°E
150°E
160°W
110°W
60°W
Pacific Ocean
Indian Ocean
Atlantic Ocean
1
2
3
4
5
6
7
8
9
10
11
12
13
14
15

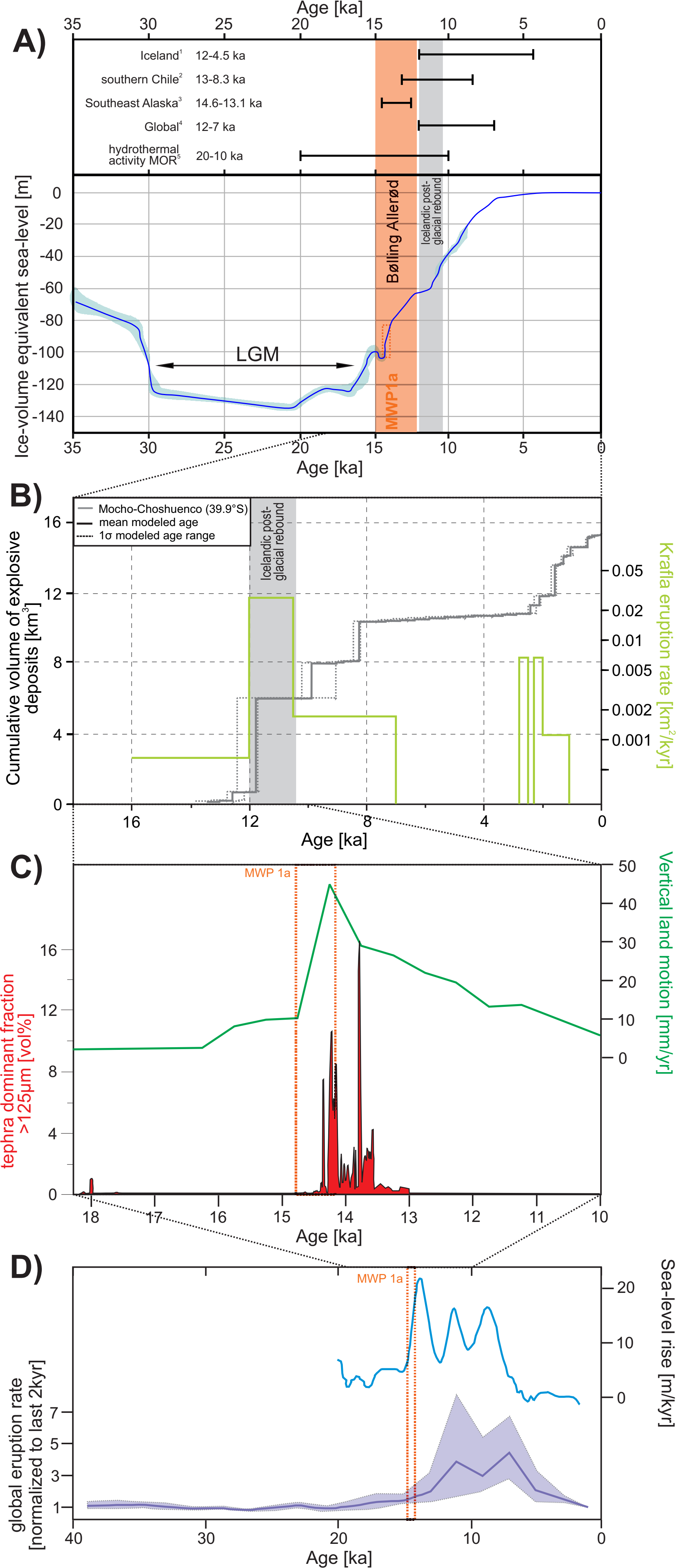

A)
Age [ka]
Iceland[1] 12-4.5 ka
southern Chile[2] 13-8.3 ka
Southeast Alaska[3] 14.6-13.1 ka
Global[4] 12-7 ka
hydrothermal activity MOR[5] 20-10 ka
Ice-volume equivalent sea-level [m]
Bølling Allerød
Icelandic post-glacial rebound
LGM
MWP1a
B)
Mocho-Choshuenco (39.9°S)
mean modeled age
1σ modeled age range
Cumulative volume of explosive deposits [km³]
Krafla eruption rate [km²/kyr]
C)
MWP 1a
tephra dominant fraction >125µm [vol%]
Vertical land motion [mm/yr]
D)
global eruption rate [normalized to last 2kyr]
Sea-level rise [m/kyr]

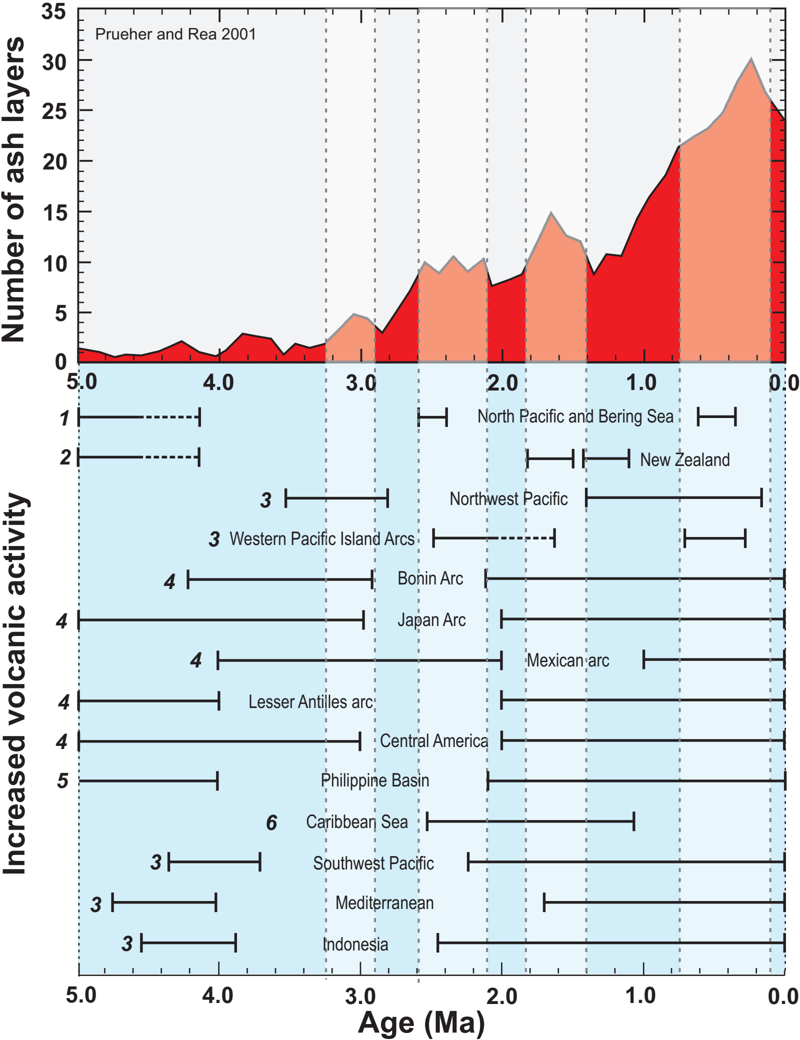

Prueher and Rea 2001
Number of ash layers
35
30
25
20
15
10
5
0
5.0
4.0
3.0
2.0
1.0
0.0
1
2
North Pacific and Bering Sea
New Zealand
3 Northwest Pacific
3 Western Pacific Island Arcs
4 Bonin Arc
4 Japan Arc
4 Mexican arc
4 Lesser Antilles arc
4 Central America
5 Philippine Basin
6 Caribbean Sea
3 Southwest Pacific
3 Mediterranean
3 Indonesia
Increased volcanic activity
Age (Ma)

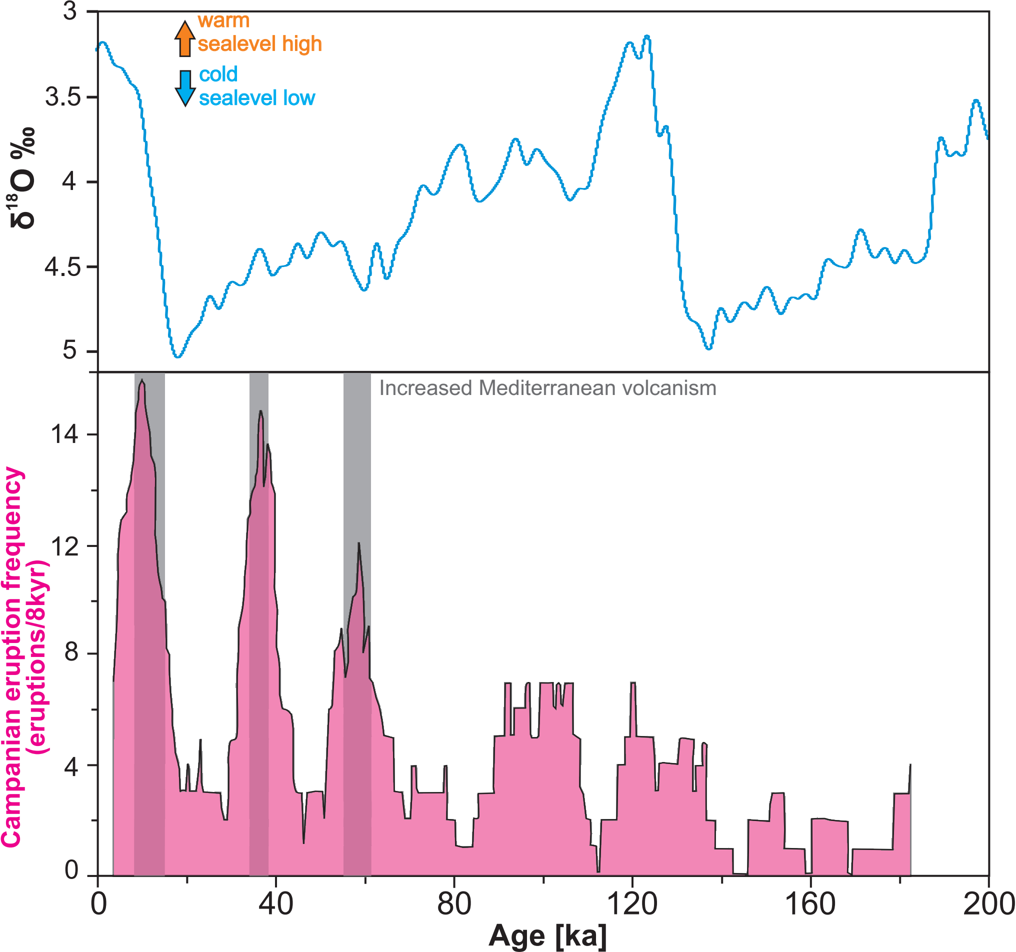

warm
sealevel high
cold
sealevel low
δ18O ‰
3
3.5
4
4.5
5
Increased Mediterranean volcanism
Campanian eruption frequency
(eruptions/8kyr)
14
12
8
4
0
0
40
80
120
160
200
Age [ka]

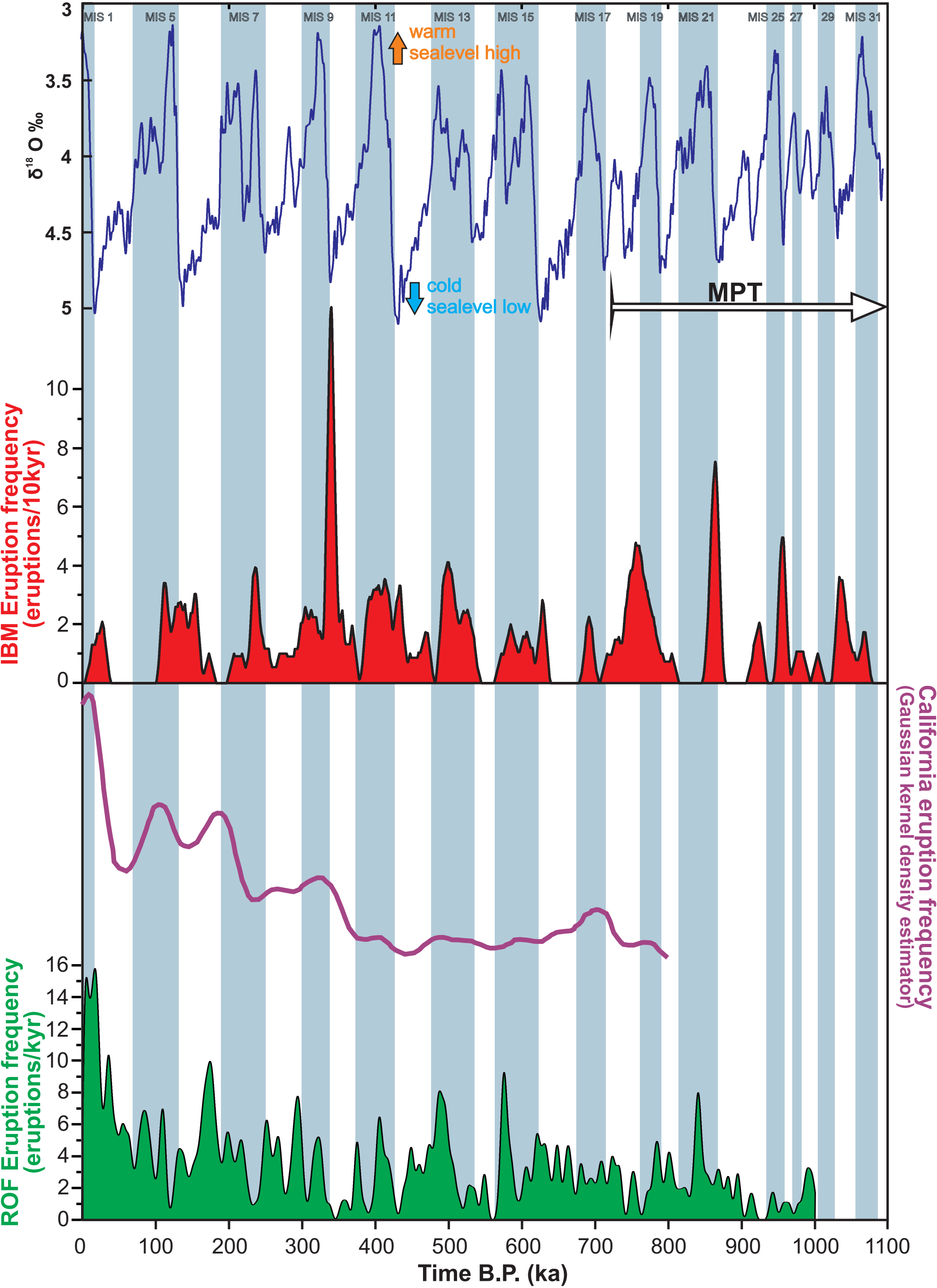

MIS 1
MIS 5
MIS 7
MIS 9
MIS 11
MIS 13
MIS 15
MIS 17
MIS 19
MIS 21
MIS 25
27
29
MIS 31
warm
sealevel high
cold
sealevel low
MPT
δ18 O ‰
IBM Eruption frequency (eruptions/10kyr)
California eruption frequency (Gaussian kernel density estimator)
ROF Eruption frequency (eruptions/kyr)
Time B.P. (ka)

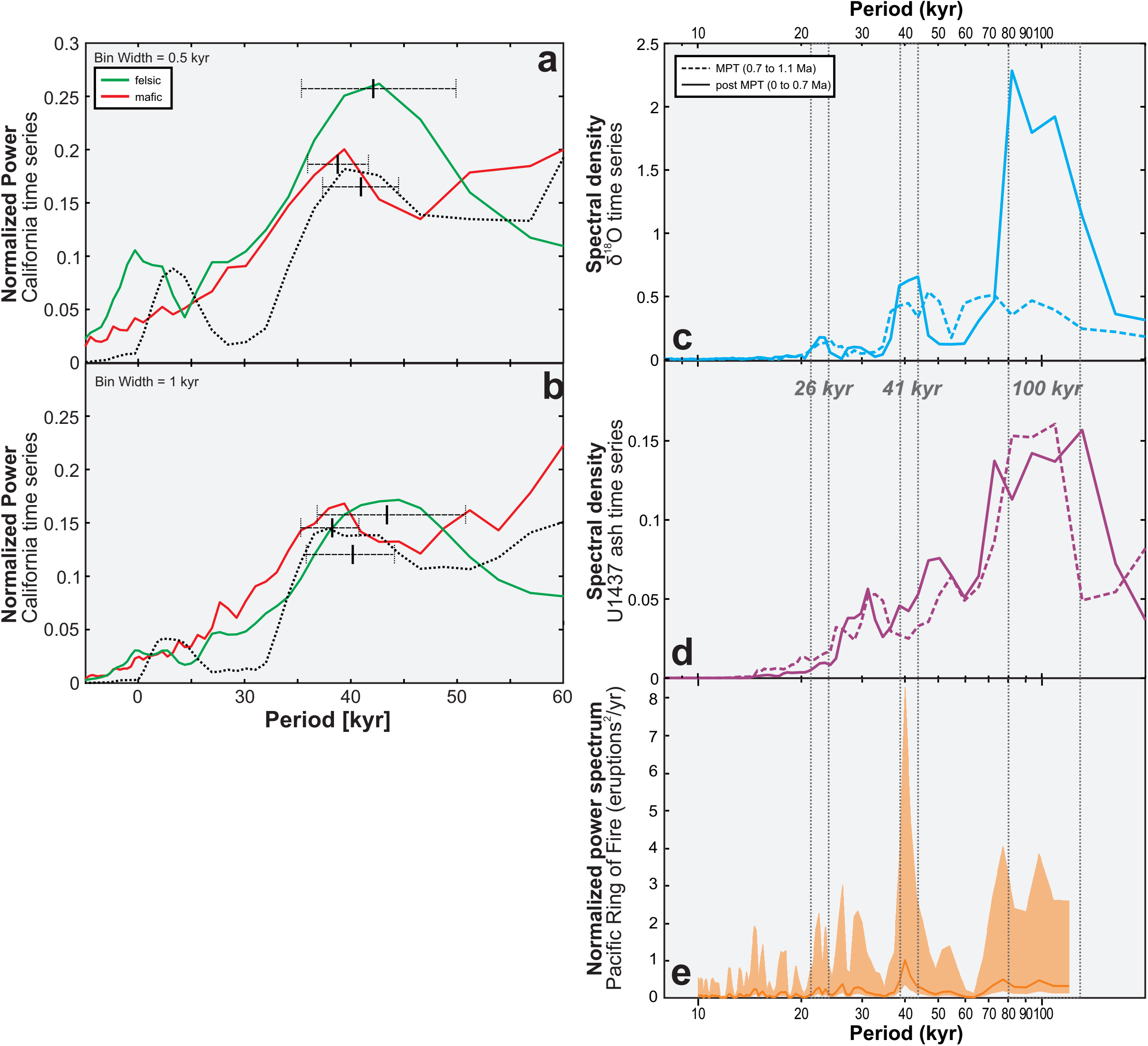

Bin Width = 0.5 kyr
felsic
mafic
a
Normalized Power
California time series
Bin Width = 1 kyr
b
Period [kyr]
Period (kyr)
MPT (0.7 to 1.1 Ma)
post MPT (0 to 0.7 Ma)
Spectral density
δ18O time series
c
26 kyr
41 kyr
100 kyr
Spectral density
U1437 ash time series
d
Normalized power spectrum
Pacific Ring of Fire (eruptions2/yr)
e

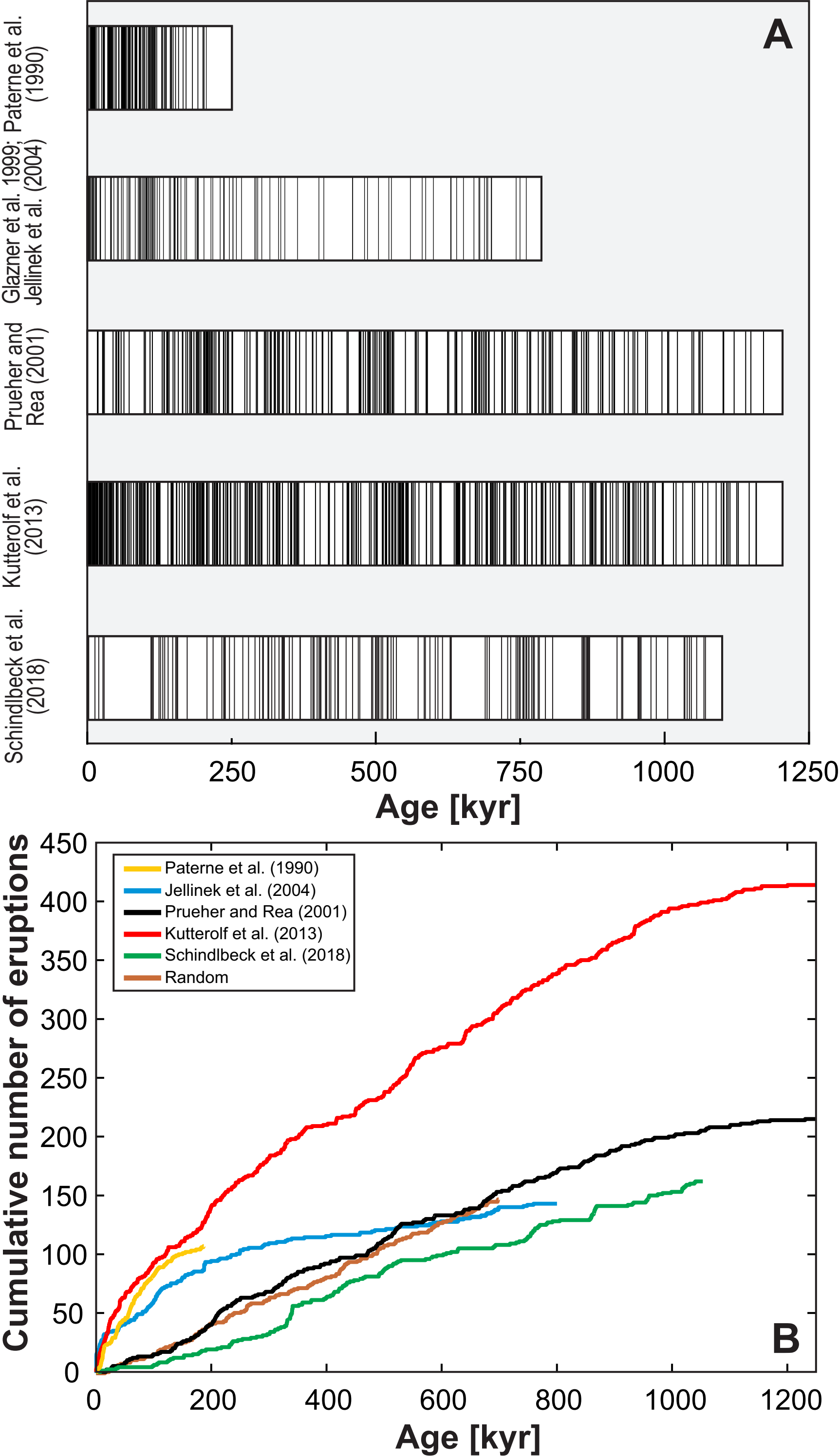
A
Paterne et al. (1990)
Glazner et al. 1999; Jellinek et al. (2004)
Prueher and Rea (2001)
Kutterolf et al. (2013)
Schindlbeck et al. (2018)
0
250
500
750
1000
1250
Age [kyr]
B
Cumulative number of eruptions
450
400
350
300
250
200
150
100
50
0
Paterne et al. (1990)
Jellinek et al. (2004)
Prueher and Rea (2001)
Kutterolf et al. (2013)
Schindlbeck et al. (2018)
Random
0
200
400
600
800
1000
1200
Age [kyr]

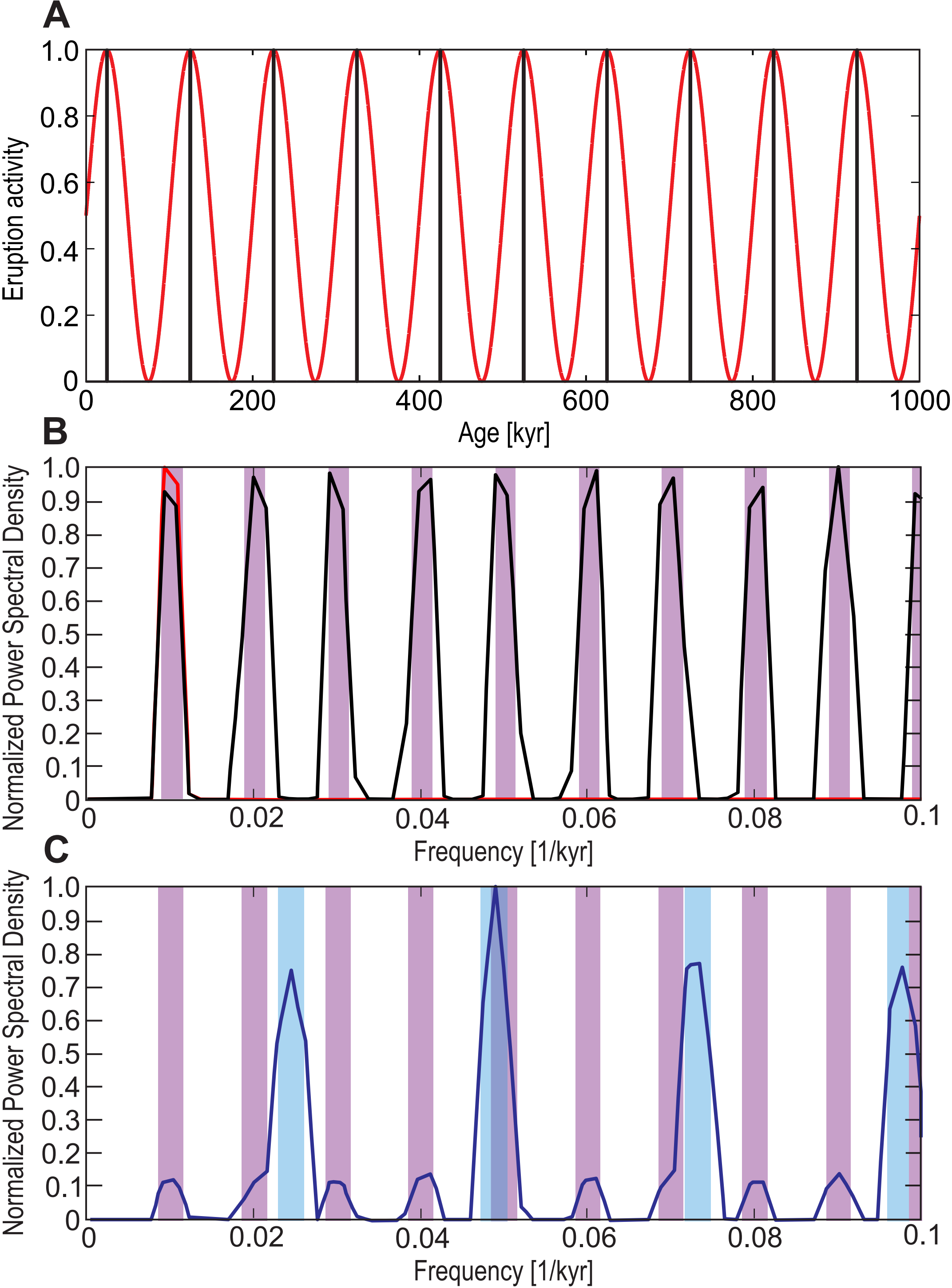

A
Eruption activity
1.0
0.8
0.6
0.4
0.2
0
0
200
400
600
800
1000
Age [kyr]
B
Normalized Power Spectral Density
1.0
0.9
0.8
0.7
0.6
0.5
0.4
0.3
0.2
0.1
0
0
0.02
0.04
0.06
0.08
0.1
Frequency [1/kyr]
C
Normalized Power Spectral Density
1.0
0.9
0.8
0.7
0.6
0.5
0.4
0.3
0.2
0.1
0
0
0.02
0.04
0.06
0.08
0.1
Frequency [1/kyr]

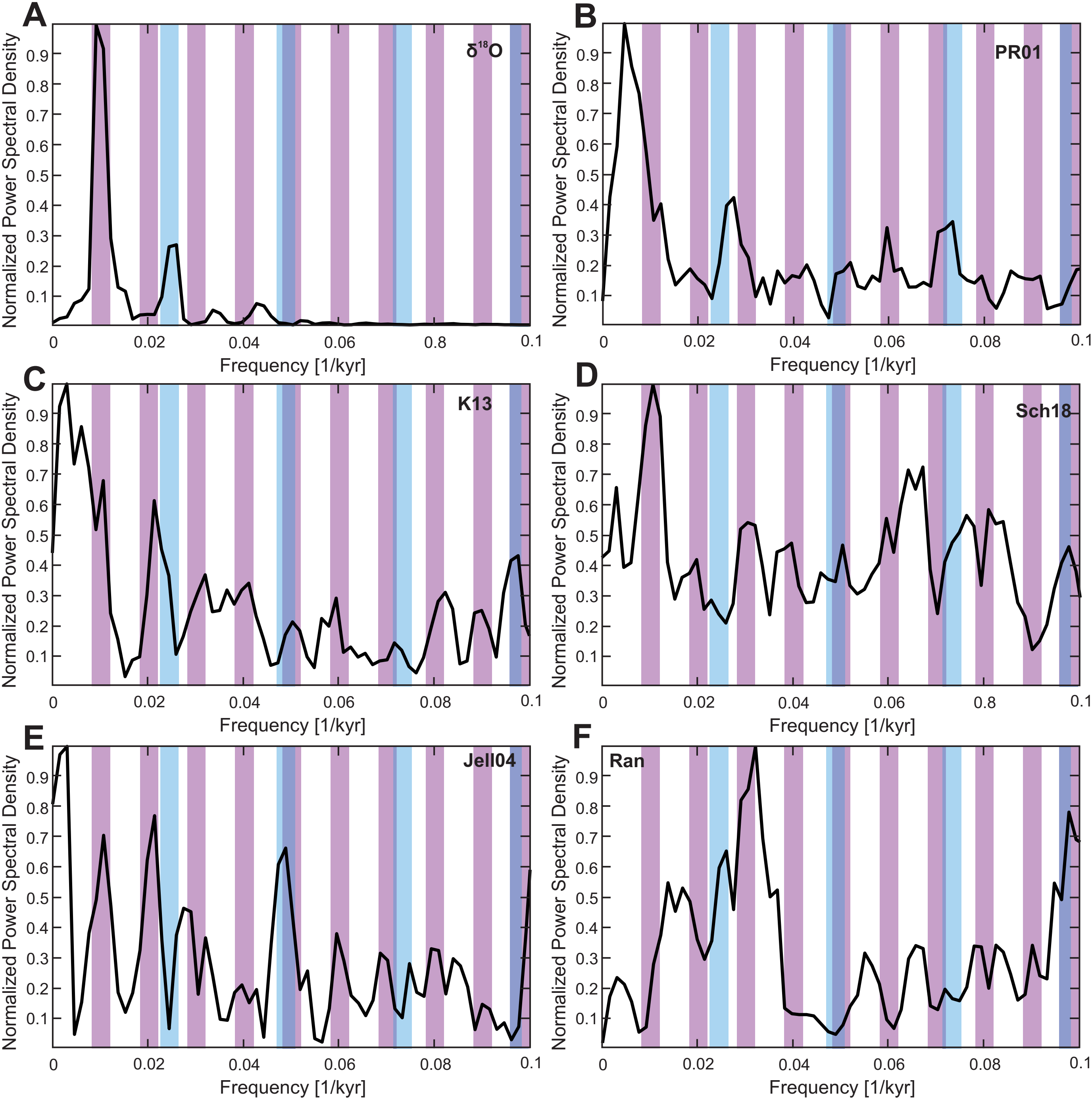

A
δ18O
B
PR01
C
K13
D
Sch18
E
Jell04
F
Ran
Normalized Power Spectral Density
Frequency [1/kyr]
0.9
0.8
0.7
0.6
0.5
0.4
0.3
0.2
0.1
0
0.02
0.04
0.06
0.8
0.1

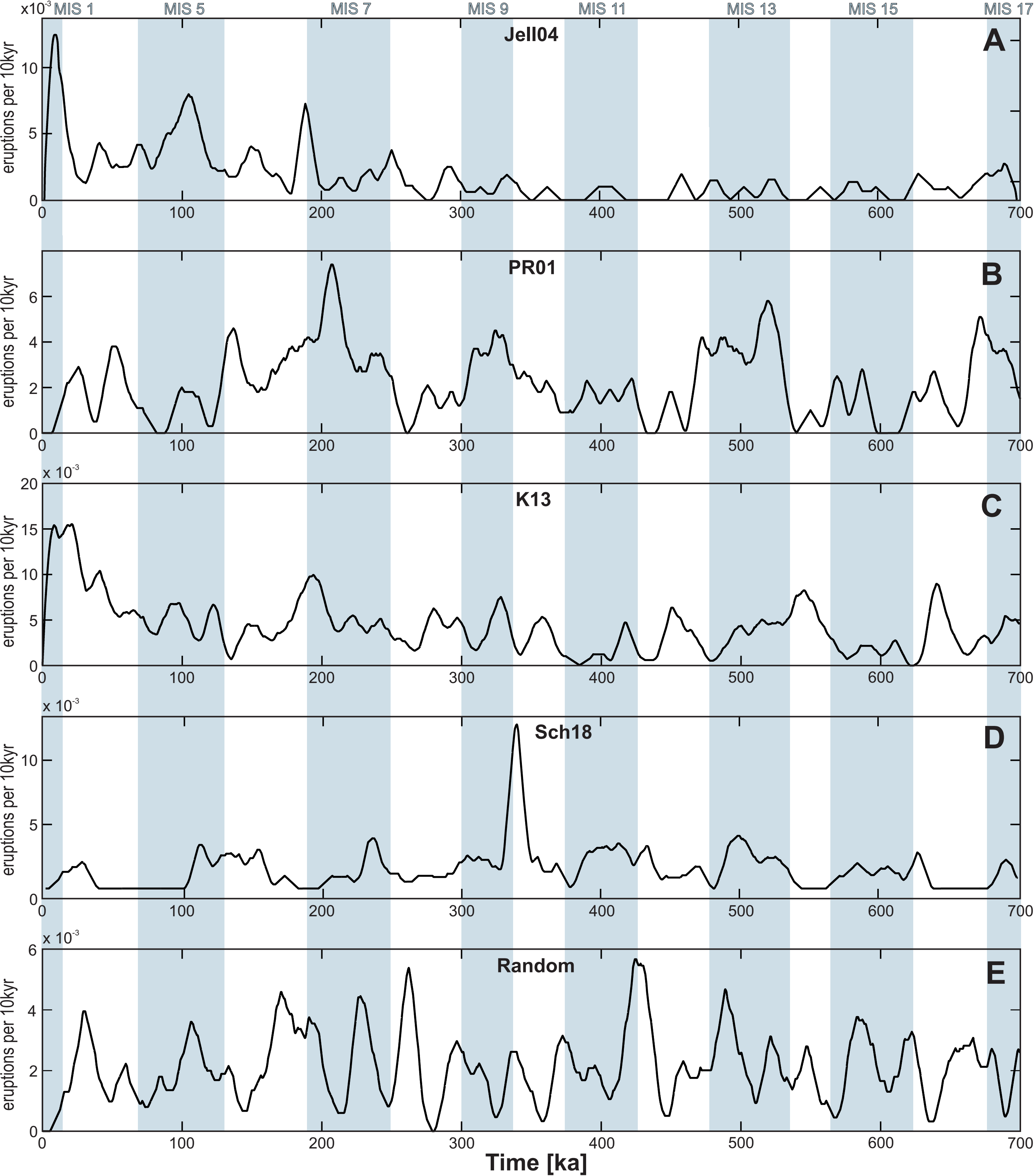

MIS 1
MIS 5
MIS 7
MIS 9
MIS 11
MIS 13
MIS 15
MIS 17
x10^-3
Jell04
A
PR01
B
x 10^-3
K13
C
x 10^-3
Sch18
D
x 10^-3
Random
E
eruptions per 10kyr
Time [ka]

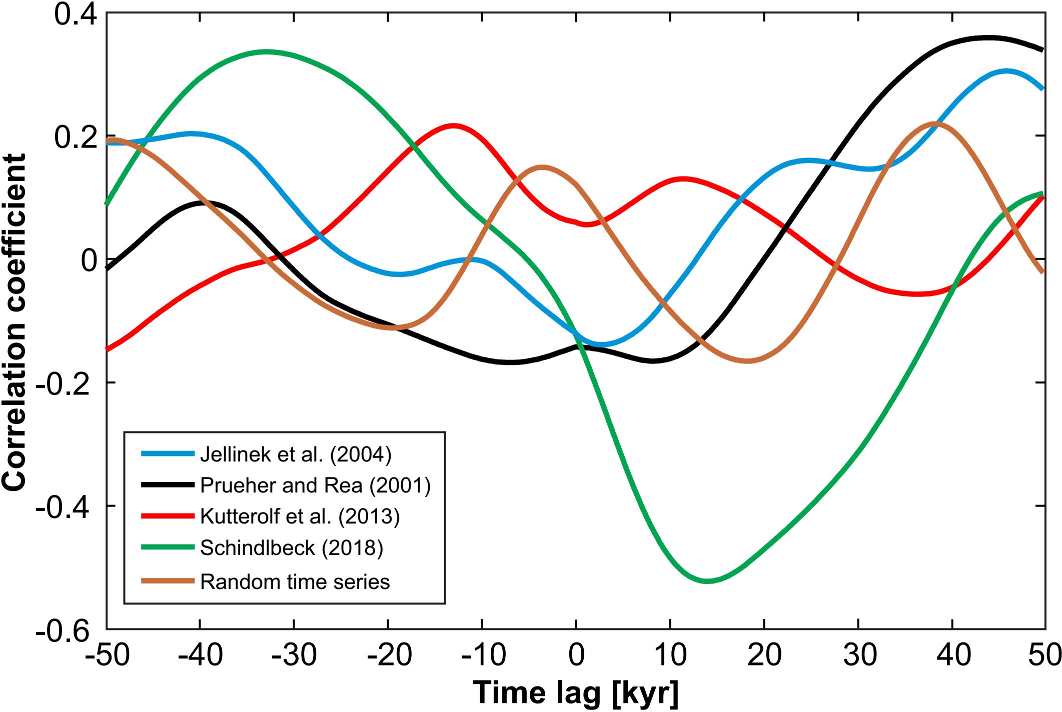

0.4
0.2
0
-0.2
-0.4
-0.6
Correlation coefficient
-50
-40
-30
-20
-10
0
10
20
30
40
50
Time lag [kyr]
Jellinek et al. (2004)
Prueher and Rea (2001)
Kutterolf et al. (2013)
Schindlbeck (2018)
Random time series

Table 1: Comparison of major parameters of selected studies on episodic and periodic volcanic activity. Entries are sorted by length of record. Numbers in column 4 refer to geographic position in Figure 2. Colors group records according to geological settings.

Study	length of time series [ka]	number of events/type of events/distribution of events	# in Figure 2	latitude (ice covered or not)	setting*	frequency/cycle/periods	suggested physical process	age dating
Rawson et al., 2016	18	75 tephras	1	yes	CIA	increase in volcanism with deglaciation	ice removal induced stress change	radiometric/age modelling
Praetorius et al., 2016	20	19 tephras	2	yes	CIA	increase in volcanism with deglaciation	stress change	sedimentation rate/radiometric/$\delta^{18}O$
Watt et al., 2013	25	121 tephra	1, 3, 4	yes/no	CIA	no or weak increase	stress change	radiometric and from Huybers and Langmuir
Huybers and Langmuir, 2009	40	5352 tephras/80% <1 ka	global	mixed	CIA	2-6 times higher during 12-7 ka deglaciation	magma production	probability distribution
McGuire et al., 1997	80	86 tephras	5	no	CIA	episodes of increased volcanism in kyr scale	stress/tectonics	sedimentation rate/radiometric/$\delta^{18}O$
Paterne et al., 1990	190	151 tephras	5	no	CIA	23 kyr	stress change	sedimentation rate/$\delta^{18}O$
Kutterolf et al., 2013	1000	408 tephras /70% <500 ka	6+ROF	mixed	OIA/CIA	41 kyr, (23, 100)	stress change	sedimentation rate
Schindlbeck et al., 2018	1100	162 tephras	7	no	OIA	100 kyr, (23, 41)	stress change	sedimentation rate/radiometric/$\delta^{18}O$
Kennett et al., 1975	2000	250 tephras	global	mixed	OIA/CIA	episodes of increased volcanism, broader focus	tectonics/climate	sedimentation rate/radiometric/$\delta^{18}O$
Prueher and Rea, 2001	5000	450 tephras	2, 3	yes	OIA/CIA	episodes of increased volcanism in Myr scale	glaciation/tectonics	paleomagnetics/sedimentati on rate
Mahony et al., 2016	15000	4936 tephras	8	no	CIA/OIA	episodes of increased volcanism in Myr scale	tectonics	sedimentation rate
Cambray and Cadet, 1994	20000	~1000 tephras	global	mixed	OIA/CIA	episodes of increased volcanism in Myr scale	stress/tectonics	sedimentation rat
Sigurdsson et al., 2000	55000	ash accumulation	9	no	OIA/CIA	episodes of increased volcanism in Myr scale	tectonics	sedimentation rate/radiometric
Sigvaldason, 1992	10	eruption rate [km^3]	10	yes	OIV	20-30 times increase during deglaciation	magma production or stress change	radiometric/stratigraphy
Maclennan et al., 2002	17	eruption rate [km^3]	10	yes	OIV	100 times increase during deglaciation	magma production	radiometric/stratigraphy
Jellinek et al., 2004	400	138 tephras	11	yes	CIV	41 kyr	stress change	radiometric
Glazner et al., 1999	800	165 tephras/85% < 400 ka	11	yes	CIV	anticorrelated volcanism and interglacial maxima	stress change	radiometric
Nowell et al. 2006	2.000	~600 ages form volc. products	12	yes	CIV	increase in volcanism with deglaciation	ice removal induced stress change	radiometric
Hasenclever et al., 2017	130	CO_2 degassing	global	submarine	MOR	5 - 15 kyr	magma production	multiple proxies, not direct
Lund and Asimov, 2011	200	chemical variation	13	submarine	MOR	increase of hyrothermal activity aftermaximal glaciation	magma production	sedimentation rate/radiometric/$\delta^{18}O$
Tolstoy, 2015	800	bathymetry	global	submarine	MOR	tidal to 100 kyr	magma production	bathymetry
Crowley et al., 2015	1250	bathymetry	14	submarine	MOR	23, 41, 100 kyr	magma production	sea level variations (models&$\delta^{18}O$)

* OIA= Ocean Island Arc, CIA= Continental Island Arc, OIV= Oceanic Intraplate Volcanism, CIV= Continental Intraplate Volcanism, MOR= Mid Ocean Ridge, ROF= Ring of Fire

Table 2: Correlation coefficients between the tephra time series spectra and a random time series spectrum. b) Probabilities of coincidental correlations between the time series; values <0.05 indicate statistically significant correlation.

a)	Kutterolf et al. 2013	Prueher and Rea 2001	Schindlbeck et al. (2018)*	Jellinek et al. 2004	Random
$\delta^{18}O$, Lisiecki and Raymo 2005	0.41	0.3	0.51	0.52	0.01
Kutterolf et al. 2013	1	0.29	0.49	0.40	0.00
Prueher and Rea 2001		1	0.31	0.28	-0.09
Schindlbeck et al. 2018			1	0.61	0.00
Jellinek et al. 2004				1	0.20
Random					1

b)	Kutterolf et al. 2013	Prueher and Rea 2001	Schindlbeck et al. (2018)*	Jellinek et al. 2004	Random
$\delta^{18}O$, Lisiecki and Raymo 2005	7.0×10^{-3}	1.3×10^{-2}	1.0×10^{-5}	9.3×10^{-2}	0.95
Kutterolf et al. 2013	1	1.3×10^{-1}	3.5×10^{-5}	9.6×10^{-4}	0.9
Prueher and Rea 2001		1	1.1×10^{-2}	2.4×10^{-2}	0.48
Schindlbeck et al. 2018			1	5.4×10^{-8}	0.6
Jellinek et al. 2004				1	0.11
Random					1